NEUROSCIENCE

# H3 acetylation selectively promotes basal progenitor proliferation and neocortex expansion

**Cemil Kerimoglu[1,2†], Linh Pham[3,4†], Anton B. Tonchev[5,6†], M. Sadman Sakib[1,2†], Yuanbin Xie[3,7], Godwin Sokpor[3,4], Pauline Antonie Ulmke[3], Lalit Kaurani[1,2], Eman Abbas[3,8,9‡], Huong Nguyen[3,10], Joachim Rosenbusch[3], Alexandra Michurina[1], Vincenzo Capece[1], Meglena Angelova[6], Nenad Maricic[11], Beate Brand-Saberi[11], Miriam Esgleas[12], Mareike Albert[9,13], Radoslav Minkov[14], Emil Kovachev[14], Ulrike Teichmann[5], Rho H. Seong[15], Wieland B. Huttner[13], Huu Phuc Nguyen[4], Anastassia Stoykova[5,16], Jochen F. Staiger[3,16], Andre Fischer[1,2,16,17]*, Tran Tuoc[3,4,16]***



**Increase in the size of human neocortex—acquired in evolution—accounts for the unique cognitive capacity of humans. This expansion reflects the evolutionarily enhanced proliferative ability of basal progenitors (BPs), including the basal radial glia and basal intermediate progenitors (bIPs) in mammalian cortex, which may have been acquired through epigenetic alterations in BPs. However, how the epigenome in BPs differs across species is not known. Here, we report that histone H3 acetylation is a key epigenetic regulation in bIP amplification and cortical expansion. Through epigenetic profiling of sorted bIPs, we show that histone H3 lysine 9 acetylation (H3K9ac) is low in murine bIPs and high in human bIPs. Elevated H3K9ac preferentially increases bIP proliferation, increasing the size and folding of the normally smooth mouse neocortex. H3K9ac drives bIP amplification by increasing expression of the evolutionarily regulated gene, *Trnp1*, in developing cortex. Our findings demonstrate a previously unknown mechanism that controls cortical architecture.**

## INTRODUCTION

The neocortex of the mammalian brain is radially structured into six neuronal layers and multiple functional domains that form the structural basis for human sensorimotor processing and intellectual ability. During embryogenesis, most cortical neurons are generated from the successive division of neural progenitor cells (NPCs) found in the forebrain germinal zones [i.e., the ventricular zone (VZ) and subventricular zone (SVZ)]. The various types of NPCs can be distinguished by their cell morphology, polarity, ability to generate a given cell lineage, and the site at which they undergo mitosis (*1*–*6*). The two main types of NPCs in the developing cortex are the apical progenitors (APs) and basal progenitors (BPs). APs include the apical/ventricular radial glia cells (a/vRGs), which divide at the surface of the apical VZ. BPs, which are derived from APs, include the basal (or outer) radial glia (bRGs) and the basal intermediate progenitors (bIPs); the latter lack apical contact and have defined mitotic activities in the inner and outer SVZs (iSVZ and oSVZ, respectively) (*1*–*6*). The aRGs and bRGs are capable of asymmetric division to self-renew and can directly or indirectly (via BPs) produce neurons (*1*–*5*, *7*).

In most lissencephalic species such as mice, most BPs are neurogenic and transient transit-amplifying bIPs (*7*, *8*). In many gyrencephalic species, such as human, BPs (including bIPs and bRGs) are capable of undergoing self-amplification through symmetric proliferative divisions before they terminally divide to generate neurons (*1*–*5*, *9*). The intricate folding (gyrification) of the human neocortex is considered to be an evolutionary adaptation to the massive expansion of neuronal populations arising from the high proliferative competence of human NPCs, especially BPs (*2*, *3*, *10*, *11*).

Recent cell sorting– and single cell–based transcriptional profiling analyses have identified a number of factors that are important for bIP proliferation, cortical expansion, and folding (*10*–*21*). Epigenomic methods have been recently established to unravel epigenetic landscapes at the single-cell level, but these strategies are limited by their low coverage of the genome and tend to cluster cells in a manner that is biased toward easily profiled genomic regions. Thus, epigenetic profiling of bIPs is still challenging, and the epigenetic mechanisms that are thought to coordinate the expression/repression of gene sets during neocortex expansion in evolution remain unexplored.

Here, we used cell sorting and a modern mass spectrometry (MS)–based epigenetic profiling to identify histone H3 lysine 9 acetylation (H3K9ac) as a key epigenetic regulation in bIP proliferation, cortical expansion, and cortical folding. We found that although the levels of H3K9ac are comparable in murine and human APs, species-specific

[1]German Center for Neurodegenerative Diseases, 37077 Goettingen, Germany. [2]Department of Psychiatry and Psychotherapy, University Medical Center, Georg-August-University Goettingen, 37075 Goettingen, Germany. [3]Institute for Neuroanatomy, University Medical Center, Georg-August-University Goettingen, 37075 Goettingen, Germany. [4]Department of Human Genetics, Ruhr University of Bochum, 44791 Bochum, Germany. [5]Max Planck Institute for Biophysical Chemistry, 37077 Goettingen, Germany. [6]Departments of Anatomy and Cell Biology and Stem Cell Biology, Research Institute, Medical University of Varna, Varna 9002, Bulgaria. [7]Department of Biochemistry and Molecular Biology, School of Basic Medical Science, Gannan Medical University, Ganzhou 341000, The People's Republic of China. [8]Zoology Department, Faculty of Science, Alexandria University, Alexandria, Egypt. [9]Center for Regenerative Therapies Dresden, Technische Universität Dresden, 01307 Dresden, Germany. [10]Faculty of Biotechnology, Thai Nguyen University of Sciences, Thai Nguyen, Vietnam. [11]Institute of Anatomy and Molecular Embryology, Ruhr University of Bochum, 44791 Bochum, Germany. [12]Institute of Stem Cell Research, Helmholtz Center Munich, German Research Center for Environmental Health, Munich, Germany. [13]Max Planck Institute of Molecular Cell Biology and Genetics, Dresden, Germany. [14]Specialized Hospital for Obstetrics and Gynecology "Prof. Dimitar Stamatov"–Varna, Medical University of Varna, Varna 9002, Bulgaria. [15]School of Biological Sciences and Institute for Molecular Biology and Genetics, Seoul National University, Seoul, South Korea. [16]DFG Center for Nanoscale Microscopy and Molecular Physiology of the Brain (CNMPB), 37075 Goettingen, Germany. [17]Cluster of Excellence "Multiscale Bioimaging: from Molecular Machines to Networks of Excitable Cells" (MBExC), Georg-August-University Goettingen, 37075 Goettingen, Germany.
*Corresponding author. Email: andre.fischer@dzne.de (A.F.); tran.tuoc@ruhr-uni-bochum.de (T.T.)
†These authors contributed equally to this work.
‡Present address: Department of Neuro- and Sensory Physiology, University Medical Center Goettingen, 37073 Goettingen, Germany.

differences exist in the histone H3 acetylation of BPs, which is low in mouse BPs and high in human BPs. Elevation of H3K9ac in the developing mouse cortex led to bIP-specific increases in the promoter H3K9ac and expression of *Trnp1*, which is a well-known regulator of NPC proliferation and cortical expansion (*11*, *22*). The experimental enhancement of H3K9ac also markedly augmented the *Trnp1* expression–dependent proliferative capacity of bIPs, leading to enlarged cortical size and folding of the developing mouse cortex. The use of an epigenome editing–based approach to increasing H3K9ac specifically at the *Trnp1* promoter resulted in increased *Trnp1* expression and bIP proliferation. Notably, the promoter H3K9ac and expression of *Trnp1* were both higher in human bIPs compared to mouse bIPs, underscoring the relevance of H3K9ac-associated *Trnp1* expression that changes in neocortical evolution. Our findings demonstrate a previously unidentified mechanism of cortical expansion during evolution and suggest that it may contribute to the formation of neocortical gyri in higher primate/human brain.

## RESULTS

### Assessing the epigenetic changes in BPs during cortical evolution

To test whether cortical expansion in evolution is correlated with alteration of the epigenetic landscape, we first investigated whether histone posttranslational modifications (PTMs) differ between T-box brain protein 2 (Tbr2)–positive (+) BPs from mouse and human cortices (Fig. 1A). To purify Tbr2$^+$ BPs from mouse and human developing cortices, we adapted a previously reported intracellular immunofluorescent staining and fluorescence-activated cell sorting (FACS) protocol (*23*, *24*). We used an antibody to label intracellular Tbr2 in single-cell suspensions isolated from E13.5 (embryonic day 13.5) and E16.5 mouse cortices and gestational week (GW) 14 and GW18 human cortices and then performed cell sorting of Tbr2$^+$ and Tbr2–negative (–) cells (Fig. 1, B and C, and fig. S1). Previous studies showed that Tbr2 is expressed in bIPs (*25*) and in a subset of Paired Box 6 (Pax6$^+$), Homeodomain-only protein homeobox (Hopx$^+$) bRGs (*26*, *27*) in the lissencephalic rodent brain. In the gyrencephalic brains of ferret and primates, TBR2 labeling was seen for bIPs and almost half of the SRY-Box Transcription Factor 2 (SOX2$^+$) and PAX6$^+$ bRG population (*28*, *29*). The expression of TBR2, however, was not found in Tenascin C (TNC$^+$), Protein Tyrosine Phosphatase Receptor Type Z1 (PTPRZ1$^+$) bRG subpopulation (*14*). Thus, the sorted Tbr2$^+$ cells from mouse and human developing cortices actually represent the majority of mouse BPs and human BPs with the latter including human bIPs and a subset of human bRGs.

A recently established MS-based method (see Materials and Methods) was applied to quantify peptides containing methylated (me) or acetylated (ac) amino acid residues (lysine, K; glutamine, Q; arginine, R) on the core histones (H2, H3, and H4) and the linker histone H1 (Fig. 1D). The levels of several epigenetic marks, predominantly modified H3 and its variants, appeared to be higher in human BPs at GW14 and GW18 than in mouse BPs at E13.5 and E16.5 (Fig. 1D, in selected frame). Some of the relevant H3 acetylation marks (Fig. 1D, red-labeled in the frame with a higher magnification shown

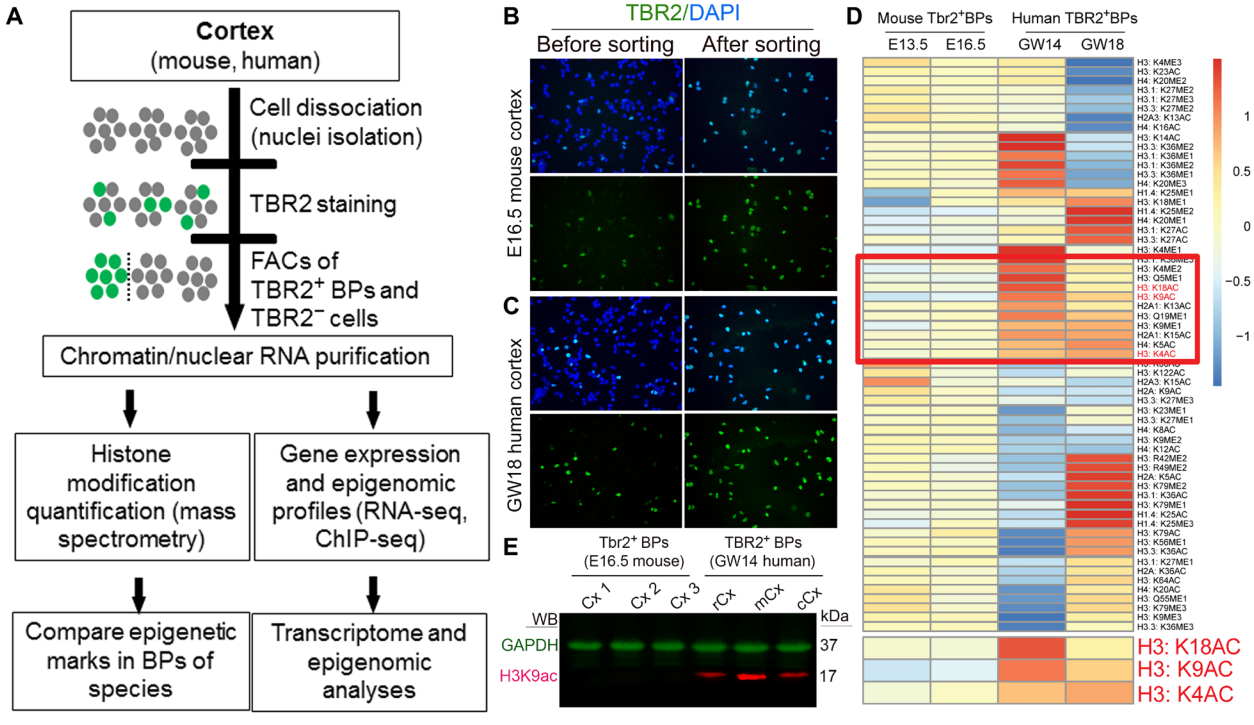


**Fig. 1. Systematic screening for epigenetic marks showing differential levels between mouse and human bIPs.** (**A**) A scheme of the experimental design used to compare the transcriptomes and epigenomes of mouse and human BPs. (**B** and **C**) Purification of Tbr2$^+$ bIPs in developing mouse and human cortex. Representative images of cell suspensions from mouse cortex (B) and human cortex (C) stained with 4′,6-diamidino-2-phenylindole (DAPI) and a Tbr2 antibody. (**D**) The data for epigenetic marks are presented as a heatmap. Bottom: Enlarged pattern showing that the levels of H3K18ac, H3K9ac, and H3K4ac are low in mouse BPs and high in human BPs. (**E**) Western blot (WB) analysis of protein extracts from Tbr2$^+$ bIPs of whole mouse cortex (Cx) and from human cortex at rostral (r), medial (m), and caudal (c) areas at indicated stages with H3K9ac antibody (in red) and with glyceraldehyde-3-phosphate dehydrogenase (GAPDH) antibody (in green, as loading control).

at the bottom), including H3K9ac, H3K18ac, and H3K4ac, were previously shown to be enriched at promoters and enhancers and to activate transcription (*30*, *31*). These findings suggest that epigenetic landscapes, particularly H3 acetylation, reflect extensive changes in BPs during cortical evolution from rodents to humans.

### Differential levels of acetylated histone H3 in BPs of developing mouse and human cortex

Among the histone acetylation marks found to differ between murine and human BPs, we selected H3K9ac for further in-depth analysis because it exhibited the highest difference between BPs from these species (Fig. 1D) and has been implicated in neuronal function, development, and plasticity (*30*, *31*). To validate the screening result, we first performed immunohistochemical (IHC) analyses with antibodies against H3K9ac and progenitor subtype markers (as indicated in the legend of Fig. 2). In E15.5 and E16.5 mouse cortices, high levels of H3K9ac (H3K9ac$^{high}$) were associated with cells in the cortical plate (CP) and the majority of Pax6$^{+}$ APs in the VZ, whereas fairly low levels of H3K9ac (H3K9ac$^{low}$) were identified in most cells of the intermediate zone (IZ) and many cells of the VZ/SVZ (Fig. 2, A and C). All Tbr2$^{+}$ BPs and 58.33 ± 17.48% Pax6$^{+}$ BPs in the SVZ and IZ were H3K9ac$^{low}$ cells (Fig. 2, A, C, and D).

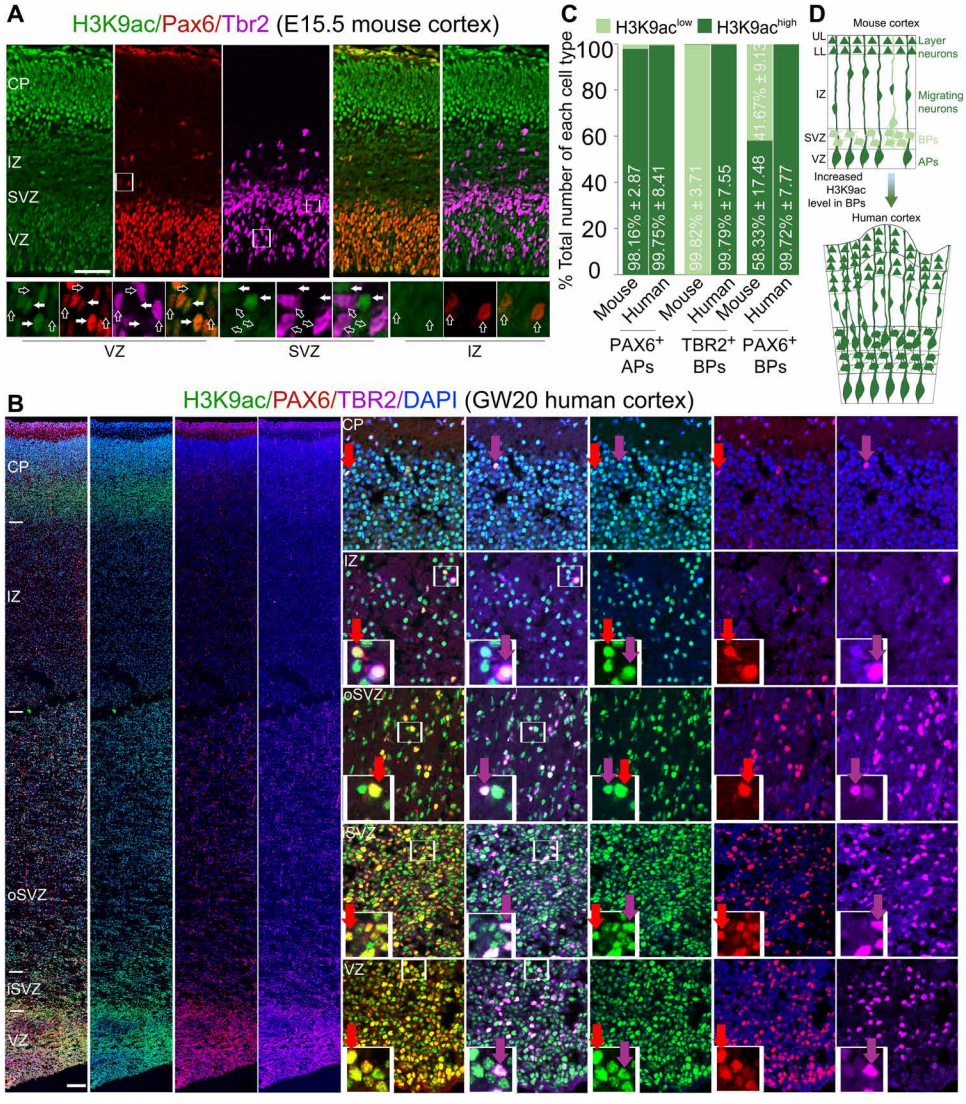


**Fig. 2. Histone H3K9 is acetylated differently in BPs in the murine and human developing cortex.** (**A**) Images of cortical sections that were obtained from E15.5 mouse embryos and subjected to triple IHC of using antibodies against H3K9ac and Pax6 (to label APs in the VZ and BPs in the IZ) and Tbr2 (to mark bIPs in the SVZ). Bottom: Higher-magnification images of the boxed areas within the VZ and IZ; they reveal that Pax6$^{high+}$ and Tbr2$^{low+}$ APs are H3K9ac$^{high+}$ cells (filled arrows), whereas Pax6$^{high+}$ BPs in the IZ and Tbr2$^{high+}$ bIPs are H3K9ac$^{low+}$ cells (hollow arrows). (**B**) Images of cortical tissue from human embryos obtained at GW20 and subjected to triple immunolabeling with antibodies against H3K9ac, Pax6, and Tbr2. Most of the Pax6$^{+}$ APs and BPs (red arrows) and the Tbr2$^{+}$ bIPs (magenta arrows) are highly immunoreactive for H3K9ac. (**C**) Statistical analyses of IHC results [shown in (A) and (B)] comparing the levels of H3K9ac (H3K9ac$^{high}$ and H3K9ac$^{low}$) in progenitor subtypes in developing mouse and human cortex. The following were compared: Pax6$^{+}$ APs in the VZ, Tbr2$^{+}$ bIPs in the VZ/SVZ, and Pax6$^{+}$ BPs in the IZ of the mouse cortex; and Pax6$^{+}$ APs in the VZ, Tbr2$^{+}$ bIPs in the VZ/iSVZ/oSVZ, and Pax6$^{+}$ BPs in the iSVZ/oSVZ of the human cortex. (**D**) Schema illustrating the higher level of H3 acetylation found in human versus mouse BPs. Scale bars, 50 μm. UL, Upper layer; LL, Lower layer.

Likewise, in the human cortex at GW20, a high level of H3K9ac was detected in the CP and in PAX6$^+$ APs (Fig. 2, B to D). In notable contrast to the mouse cortex, most PAX6$^+$ BPs and TBR2$^+$ BPs in the human iSVZ and oSVZ were H3K9ac$^{high}$ cells (Fig. 2, B to D). The difference in the H3K9ac levels of mouse and human TBR2$^+$ BPs was also confirmed by Western blot (WB) analysis with lysates from FACS-collected Tbr2$^+$ cells (Fig. 1E).

To determine whether the detected difference in the H3 acetylation levels of the two species was restricted to K9 or also present on other amino acid residues, we examined the pan-acetylation of H3 (H3ac) (fig. S2). Triple IHC analysis of cortical tissues from E15.5 mouse and GW20 human embryos showed that, in the mouse cortex, H3ac is highly expressed in PAX6$^+$ APs, but not in TBR2$^+$ BPs. In the human cortex, however, PAX6$^+$ APs in the VZ and PAX6$^+$/TBR2$^+$ BPs in the iSVZ and oSVZ showed high-level H3ac expression (fig. S2, A to C). Notably, numerous KI67$^+$ cycling progenitors were H3ac$^{low/negative}$ and H3K9ac$^{low/negative}$ cells, suggesting that the elevation of H3ac and H3K9ac is not common to all progenitors in human cortex (fig. S2, D and E).

Our gene ontology (GO) analysis for RNA sequencing (RNA-seq) data of Tbr2$^+$ BPs versus Tbr2$^-$ cells revealed high expression of many genes encoding for proteins with deacetylase activity, especially histone deacetylases (Hdacs) (such as Hdac1, Hdac2, Hdac3, Hdac8, and Hdac9; fig. S2, F to H). This observation suggests that the high expression of Hdacs might remove H3K9ac and possibly other H3ac(s) in Tbr2$^+$ BPs in developing mouse cortex. As histone H3 is acetylated more highly in human BPs than in mouse BPs, we designed experiments to elucidate the in vivo outcome of increased H3ac levels using Hdac inhibition and overexpression of the H3K9 acetyltransferase, Lysine Acetyltransferase 2A (Kat2A)/Gcn5, during mouse cortical development.

## Increased H3 acetylation promotes the generation of BPs

We first tested whether increased acetylation of H3 could increase the genesis and proliferation of BPs in mice. To elevate H3ac, we administered trichostatin A (TSA), which is a selective class I/II Hdac inhibitor (Hdaci), to embryos from control [wild-type (WT)] mice (Fig. 3A). We previously showed that the cortex-specific loss of BRG1-Associated Factor 155 (Baf155), as seen in BRG1-Associated Factor 155 conditional knockout (Baf155cKO) embryos, promoted delamination of APs, increasing the population of Pax6$^+$ and Tbr2$^+$ BPs in the IZ and diminished the pool of Pax6$^+$ APs in the VZ [control + vehicle (Veh) and Baf155cKO + Veh; see also Fig. 3, B and C] (*32*). As Pax6$^+$ bRGs are relatively rare in the WT mouse cortex (*26*, *27*), we used the Baf155cKO mutant as a mouse model to investigate the effect of Hdac inhibition on the proliferation of BPs. TSA was injected daily beginning at 12.5 days post coitum (d.p.c.), and WT and Baf155cKO embryos were examined at E16.5 to E18.5 (Fig. 3A). TSA treatment had no major effect on the pool of Pax6$^+$/Activating Enhancer-Binding Protein 2 Gamma (Ap2γ$^+$)/Sox2$^+$ APs in the VZs of WT and Baf155cKO mutants when compared to the corresponding Veh-treated controls (Fig. 3, B and C). TSA injection increased the numbers of Pax6$^+$/Ap2γ$^+$/Sox2$^+$/Tbr2$^+$ BPs in the SVZ/IZ (Fig. 3, B and C, left) of WT mice and more pronouncedly in Baf155cKO embryos (Fig. 3, B and C, right).

Triple IHC analysis of Pax6, Tbr2, and Ki67 at E16.5 and E18.5 revealed that inhibition of Hdac leads to regionally restricted increases in Tbr2$^+$, Pax6$^+$, and Ki67$^+$ BPs in sections taken from the rostral, middle, and caudal dorsolateral cortex (d/lCx), but not the medial cortex (mCx) (fig. S3). Hdac inhibition exerted a dose-dependent effect, as more Tbr2$^+$/Pax6$^+$ BPs were found in E18.5 cortex treated with TSA for 6 days (E12.5 to E17.5) compared to those of embryos treated for only 3 days (E12.5 to E15.5) (fig. S4, A and B). Most Tbr2$^+$ BPs of the WT cortex were previously reported to be negative for Pax6 immunostaining (*25*). The proportion of cortical progenitors expressing both Pax6 and Tbr2 was high in TSA-treated cortex (fig. S4C), as also reported in the developing gyrencephalic neocortex (*28*, *29*).

Whereas only a few Pax6$^+$/Phosphorylated vimentin (pVim$^+$) cells with basal processes characteristic of BPs/bRGs are found in the Veh-treated cortex, they were frequently seen in the TSA-treated mouse cortex (Fig. 3, D to G). The basal processes of Pax6$^+$ cells in SVZ/IZ were also marked by 1,1′-dioctadecyl-3,3,3′,3′-tetramethylindocarbocyanine perchlorate (DiI) labeling and by retroviral green fluorescent protein (GFP) protein. Notably, TSA treatment resulted in increased numbers of Pax6$^+$/pVim$^+$ BPs with the highest numbers found in TSA-treated Baf155cKO cortex (Fig. 3G). In addition, proteins enriched in a/bRG cells, such as Tnc, Ptprz1, and Hopx (*14*, *27*), were also highly expressed in a subset of Pax6$^+$/Tbr2$^-$ a/bRG cells from TSA-treated mouse cortex (Fig. 3, H to J, and fig. S8).

To further confirm that the genesis of BPs is increased in Hdac inhibition, we treated pregnant mice with agents whose properties are similar to TSA; these included valproic acid (VPA) and suberoylanilide hydroxamic acid (SAHA), which also inhibit class I/II Hdacs. Both VPA- and SAHA-treated developing cortices had more BPs than Veh-treated cortex [fig. S5; see also Fig. 7H and fig. S10 (G and H) for cortical phenotype of the H3K9 acetyltransferase Kat2a overexpression], supporting the idea that the Hdac inhibition–induced elevation of H3 acetylation directly contributes to increasing the generation of BPs.

## Increased H3 acetylation preferentially enhances the proliferation of BPs but not APs

The presence of more BPs in TSA-treated Baf155cKO cortex (Fig. 3, A to C) suggested that the delaminated progenitors undergo self-amplification in response to enhanced H3 acetylation. To ascertain whether H3 acetylation is important for the proliferation of cortical progenitors (APs and BPs), we examined their proliferative capacity by performing IHC with antibodies against Pax6, Tbr2, and phosphorylated histone H3 (pHh3) (Fig. 4, A and B). On the basis of the expression of Pax6 in the VZ and pHh3 at the apical VZ surface (Fig. 4, A and C), our data suggest that TSA injection did not influence the proliferation of APs, which already have a high endogenous level of acetylated H3. Notably, upon Hdaci treatment, both control and Baf155cKO cortices presented more nonapical proliferating (pHh3$^+$ BPs) cells, along with higher ratios of proliferating Tbr2$^+$/pHh3$^+$ BPs to total Tbr2$^+$ cells and proliferating Pax6$^+$/pHh3$^+$ BPs to total Pax6$^+$ BPs (Fig. 4, A to C). Consistent with these data, the number of actively cycling BPs (Ki67$^+$/Tbr2$^+$; Ki67$^+$/Pax6$^+$) in the SVZ/IZ was considerably increased in TSA-treated Baf155cKO cortex (Fig. 4, D and E).

In addition to the lengthened cell cycle in neural progenitors from primate than that from rodent (*3*), both proliferative APs and BPs exhibit a substantially longer S phase than neurogenic progenitors (*33*). We therefore focused on examining the effect of TSA on progression from S phase to $G_2$-M phases in APs and BPs. Given that the average lengths at midgestation stage of the S phase and $G_2$-M cell cycle phases are about 3.5 and 2 hours, respectively (*33*), we then examined whether the TSA treatment affected the progression within S-$G_2$-M phases in APs and BPs. A thymidine analog injection paradigm [4-hour 5′-iododeoxyuridine (IdU) pulse labeling] was

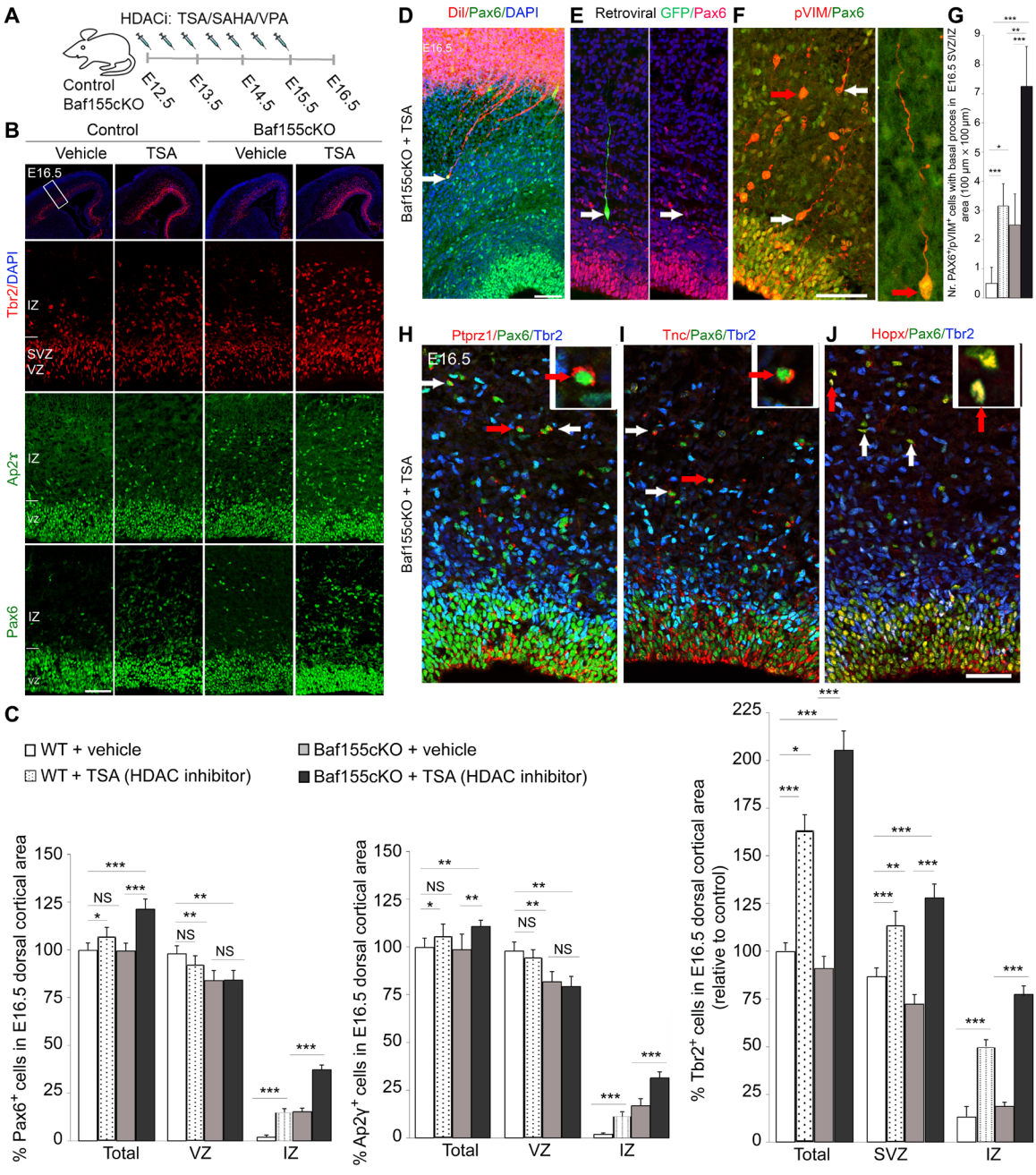


**Fig. 3. Enhanced acetylation of H3 increases the number of BPs.** (**A**) Experimental paradigm in which Baf155cKO and control embryos were treated with Hdacis [TSA, SAHA (suberoylanilide hydroxamic acid), and VPA (valproic acid)] at the indicated developmental stages. (**B**) IHC images showing Tbr2 (bIPs), Pax6 (APs and BPs), and Ap2γ (APs and BPs) in sections from control and Baf155cKO embryos with or without TSA treatment. (**C**) Statistical comparisons indicate that increased H3 acetylation enhanced the number of BPs ($Tbr2^+$, $Pax6^+$, and $Ap2\gamma^+$ cells of the IZ) in TSA-treated WT and Baf155cKO embryos compared to Veh-treated controls. (**D** to **F**) Confirmation of BPs/bRGs (arrows) based on their morphology. BPs/bRGs exhibit long basal processes but no apical processes in TSA-treated cortex, as revealed by double labeling of Pax6 with 1,1′-dioctadecyl-3,3,3′,3′-tetramethylindocarbocyanine perchlorate (DiI) (D), retroviral green fluorescent protein (GFP) (E), or pVim (F). Notably, fanned fibers of $Pax6^+$ BPs/bRGs were observed when DiI labeling was applied at the pia (D). (F) High-magnification image of a $Pax6^+/pVim^+$ BPs/bRG indicated by a red arrow. (**G**) Statistical analysis comparing number of $Pax6^+/pVim^+$ BPs/bRGs with basal processes in the SVZ/IZ of the indicated embryos. (**H** and **I**) IHC analysis shows the expression of the human-enriched bRG markers, Ptprz1 (H), Tnc (I), and Hopx (J) in $Pax6^+/Tbr2^-$ cells (arrows) of TSA-treated Baf155cKO cortex at E16.5 (see also fig. S8 for E18.5 cortex). Values are presented as means ± SEMs (*$P < 0.05$, **$P < 0.01$, and ***$P < 0.005$). NS, not significant. Scale bars, 50 µm.

used to mark cortical progenitors within these phases. We performed double immunostaining with antibodies against IdU and pHh3 to label APs (apical surface–located $IdU^+/pHh3^+$) and BPs (basally located $IdU^+/pHh3^+$), which already entered G-M phases (fig. S6, A and B). Fewer BPs (but not APs) reached late $G_2$-M phases in TSA-treated cortices compared to Veh-treated cortices. This implicated that TSA treatment resulted in lengthening of cell cycle progression in S-$G_2$-M phases in BPs specifically. Together,

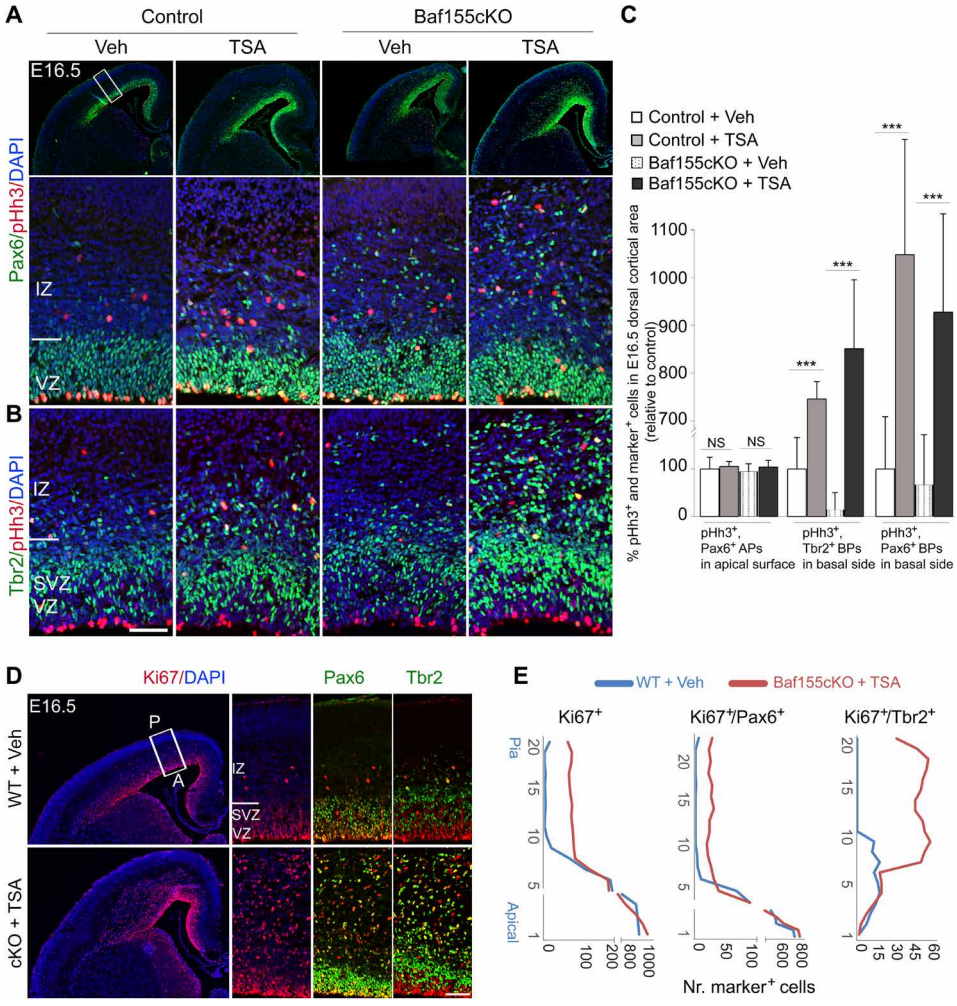


**Fig. 4. H3 acetylation specifically promotes proliferation of BPs in developing mouse cortex.** (**A** and **B**) Images showing double IHC of Pax6/pHh3 and Tbr2/pHh3 in control or Baf155-deficient cortex treated with Veh or Hdaci, as assessed at E16.5. Bottom: Higher magnifications of the areas indicated by the white box. (**C**) Statistical analyses reveal that elevated acetylation of H3 causes a notable increase in the number of $Tbr2^+/pHh3^+$ bIPs and $Pax6^+/pHh3^+$ BPs, whereas the number of apical $Pax6^+/pHh3^+$ APs cells is not affected. (**D**) IHC images for Ki67/Pax6 or Ki67/Tbr2 staining of Veh-treated WT and TSA-treated Baf155cKO cortex at E16.5. Right: Higher magnifications of the areas indicated by the white box. (**E**) Quantified distribution of proliferating $Ki67^+/Pax6^+$ APs/BPs and $Ki67^+/Tbr2^+$ bIPs from the apical surface to the pia in Veh-treated WT cortex and the corresponding region of the TSA-treated Baf155cKO cortex shown in (A). Values are presented as means ± SEM (***$P < 0.005$). Scale bars, 50 μm.

these data indicate that the proliferative capability of murine BPs is enhanced by elevated acetylation of H3.

### Identification of H3K9ac target genes in $Tbr2^+$ BPs

Given that TSA treatment had a much stronger effect on BP genesis in Baf155cKO cortex, we first compared the gene expression and genome-wide H3K9ac profiles of TSA- and Veh-treated Baf155cKO cortices by RNA-seq and chromatin immunoprecipitation sequencing (ChIP-seq) (Fig. 5, A and B, and tables S1 and S2). We found that TSA treatment yielded up-regulation of 1961 genes and down-regulation of 1799 genes ($P < 0.01$ and $|\text{fold change}| > 1.2$) (Fig. 5A and table S1). Examination of H3K9ac on the TSA-regulated genes revealed that the up-regulated genes had clear increases in the level of H3K9ac (fig. S7A), whereas the down-regulated genes did not show any substantial change in H3K9ac (fig. S7B). This result is in accordance with data showing that loss of H3K9 acetyltransferases can trigger activation of a set of genes via secondary effects (*34*).

In accordance with our IHC data showing an increase in the number of $Tbr2^+/Pax6^+$ BPs, many neurogenic BP/bIP genes (e.g., *Neurog1*, *Neurog2*, *Eomes/Tbr2*, *Neurod2*, and *Neurod6*) were up-regulated in the cortex of TSA-injected Baf155cKO mutants (Fig. 5A and table S1). TSA treatment also yielded increased expression of genes previously shown to be enriched in BPs/bRGs (e.g., *Tnc*, *Ptprz1*, *Paqr8*, *Gigyf2*, *Pdlim3*, and *Zc3hav1*; fig. S8A and table S1) (*14*). The increased expression of many BP-enriched genes in response to Hdac inhibition in both Baf155cKO and WT cortices was also confirmed by quantitative polymerase chain reaction (qPCR) and IHC analyses (figs. S7C and S8). Furthermore, the results from our ChIP-seq and ChIP/qPCR analyses also confirmed that many of the BP genes (e.g., *Tnc*, *Paqr8*, *Neurog2*, *Eomes*, *Neurod1*, and *Neurod6*; fig. S7D and table S2) exhibited increases in their H3K9ac levels in the cortices of TSA-treated Baf155cKO and WT embryos. These findings indicated that H3 acetylation positively regulates the expression of BP genes.

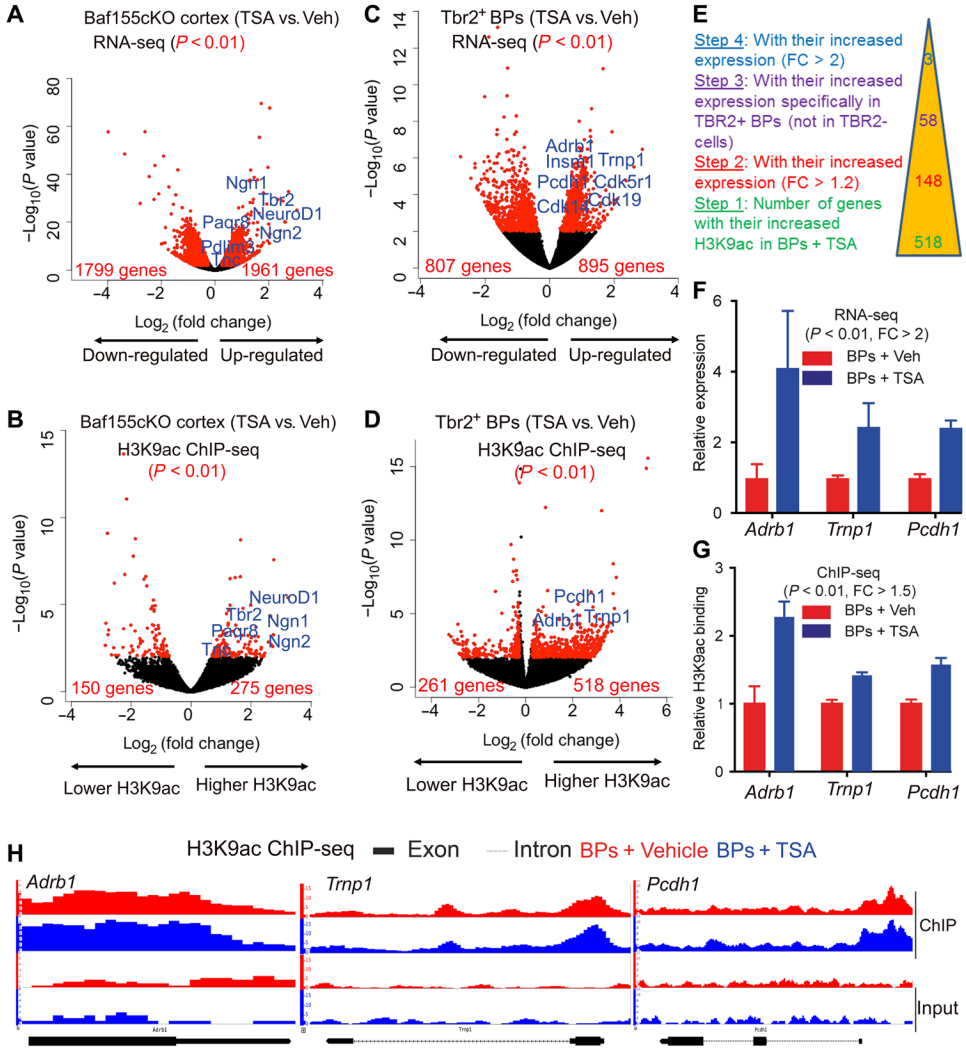


**Fig. 5. Identification of H3K9ac target genes in Tbr2$^+$ bIPs.** (**A** to **D**) Volcano plots showing statistically significant changes [paired Student's *t* test $P < 0.01$, fold change (FC) > 1.2] visualized by our RNA-seq (A and C) and H3K9ac ChIP-seq (B and D) analyses of E16.5 Baf155cKO cortex (A and B) and Tbr2$^+$ BPs (C and D) in TSA versus Veh experiments [see also fig. S7 (E and F) for Tbr2$^-$ cells]. (**E**) Stepwise exclusion parameters were applied to the H3K9ac ChIP-seq and RNA-seq datasets to search for genes specifically activated by H3K9ac in Tbr2$^+$ BPs. (**F**) The expression levels of *Adrb1*, *Trnp1*, and *Pcdh1* are up-regulated in TSA-treated BPs. (**G** and **H**) Level of H3K9ac (G) and distribution of H3K9ac along the gene bodies (H) of *Adrb1*, *Trnp1*, and *Pcdh1* in TSA-treated bIPs (red) and Veh-treated BPs (blue). Input (bottom row) and distributions after immunoprecipitation (top two rows) are depicted.

Next, we evaluated the TSA treatment response of Tbr2$^+$ bIPs (Fig. 5, C and D and tables S3 and S4) and Tbr2$^-$ cells (fig. S7, E and F, and tables S5 and S6). For this purpose, Tbr2$^+$ and Tbr2$^-$ nuclei were sorted by FACS (Fig. 1 and fig. S1). TSA treatment yielded expressional up-regulation of 895 genes in Tbr2$^+$ bIPs. To provide additional evidence that H3 acetylation induces expression of bIP genes during evolution, we compared the up-regulated genes in TSA-treated Tbr2$^+$ bIPs with bIP genes that were recently identified to be specific for macaque or human (*35*). TSA treatment provoked expression of 40.1% (166 of 414) macaque-specific BP genes and 13.3% (62 of 467) human-specific BP genes in Tbr2$^+$ BPs in the developing mouse cortex (fig. S7, G and H, and table S7), suggesting that H3 acetylation has an evolutionary relevance in BP genesis during mammalian evolution. Among the up-regulated genes in TSA-treated Tbr2$^+$ BP genes, 37 showed correlation between their up-regulation and an increased level of H3K9ac upon TSA treatment ($P < 0.01$; fig. S7I and table S4). Unexpectedly, neither the H3K9ac level nor the expression levels of typical BP genes (e.g., *Eomes*, *Neurog1*, *Neurog2*, *Neurog1*, and *Neurod4*) were found to be altered in TSA-treated BPs (fig. S7J and tables S3 to S6). Thus, the up-regulated expression of most typical BP genes in TSA-treated developing mouse cortex seems to be a secondary effect.

The increased proliferation of bIPs, which was visualized as increases in Tbr2$^+$/pHh3$^+$ and Tbr2$^+$/Ki67$^+$ cells (Fig. 4), suggested that the expression of proliferation-related genes would be increased. We found that the expression levels of cell cycle genes (e.g., *Cdk19*, *Cdk5r1*, and *Cdk14*) and *Insm1*, which is known to promote bIP proliferation, were up-regulated in TSA-treated bIPs (Fig. 5C and table S3). However, the levels of H3K9ac at the promoters of these genes were not increased following TSA treatment (Fig. 5D and table S4). These findings suggested that TSA treatment might influence

the expression of factors that act upstream of the aforementioned proliferation-regulated genes.

To identify candidates for functional analysis, we undertook an unbiased approach. From among all genes that exhibited increased H3K9ac at their promoters in Tbr2$^+$ bIP cells after TSA injection (|fold change| > 1.2; Fig. 5E), we selected those that also showed a trend for increased expression (|fold change| > 1.2; Fig. 5E). This screen netted 148 genes (Fig. 5E). From them, we filtered out those that exhibited increased expression in Tbr2$^-$ cells, yielding 58 genes that had increased H3K9ac and were uniquely up-regulated in Tbr2$^+$ bIP cells following TSA treatment (Fig. 5E). These genes were further filtered according to their basal expression levels (baseMean > 20) and selection of those that increased by more than twofold. This pipeline yielded three candidates: *Adrb1*, *Trnp1*, and *Pcdh1* (Fig. 5, F and H, and fig. S7K). This suggests that H3 acetylation promotes bIP amplification by directly activating the expression of a small set of genes.

### H3 acetylation controls the amplification of bIPs by regulating *Trnp1* expression in the developing cortex

In the developing mouse cortex, *Trnp1* is exclusively localized in the nuclei of APs in the VZ and nascent neurons in the CP with little to no *Trnp1* expression seen among Tbr2$^+$ bIPs in the SVZ (Fig. 6A) (*11*); it thus exhibits a pattern similar to that of H3K9ac (Figs. 1E and 2). In line with this, the expression and promoter H3K9ac levels of *Trnp1* were lower in Tbr2$^+$ bIPs than in Tbr2$^-$ cells of the developing mouse cortex, as revealed by our RNA-seq and ChIP-seq experiments (fig. S9, A and B). Notably, the expression (Fig. 6, A and B) and promoter H3K9ac (Fig. 6C and fig. S9C) levels of *Trnp1* were notably higher in human TBR2$^+$ bIPs than in mouse Tbr2$^+$ bIPs. These data suggest that the H3K9ac level directly controls the expression of *Trnp1* (also see the model in Fig. 7I). This proposal was further corroborated by our observation that *Trnp1* expression is increased specifically in Tbr2$^+$ cells upon TSA treatment (fig. S9, D and E).

To more directly investigate whether a higher level of H3K9ac at the *Trnp1* locus might enhance the gene expression and proliferation of bIPs in the mouse developing neocortex, we sought to increase H3K9ac at the *Trnp1* locus and examine the associated phenotype. To increase deposition of the H3K9ac mark, we adapted a CRISPR-dCas9–based system (*36*) that allows targeted editing of H3K9ac in the developing cortex (Fig. 6D). Given that the levels of H3K9ac at the *Trnp1* promoter differed between mouse Tbr2$^+$ bIPs and human TBR2$^+$ bIPs (Fig. 6C) and between mouse Tbr2$^+$ bIPs and Tbr2$^-$ cells (fig. S9B) and TSA treatment increased H3K9ac at the *Trnp1* promoter specifically in bIPs (fig. S9, D and E), we selected the *Trnp1* promoter for targeted H3K9ac editing. Several guide RNAs (gRNAs) targeting the *Trnp1* promoter were designed and tested (fig. S9, F and G). To edit histone acetylation at the *Trnp1* locus, we generated plasmid constructs (g*Trnp1*-dCas9-Kat2a-T2A-eGFP) harboring DNA sequences that encoded a gRNA, dCas9 (a nuclease-deficient Cas9) fused with an H3K9ac writer Kat2a, and a fluorescent reporter (GFP) (Fig. 6D). Two gRNA-expressing constructs (gRNA#2 and gRNA#4), designated as g*Trnp1*, were used to target the *Trnp1* locus (fig. S9, F and G).

To validate that H3K9ac levels changed upon introduction of g*Trnp1*, we carried out ChIP-qPCR experiment using FACS-purified transfected (GFP$^+$) Neuro2A cells. H3K9ac levels were observed to have increased substantially at the *Trnp1* promoter region upon g*Trnp1* transfection compared to control conditions (fig. S9H). In addition, qPCR analysis of the sorted cells revealed

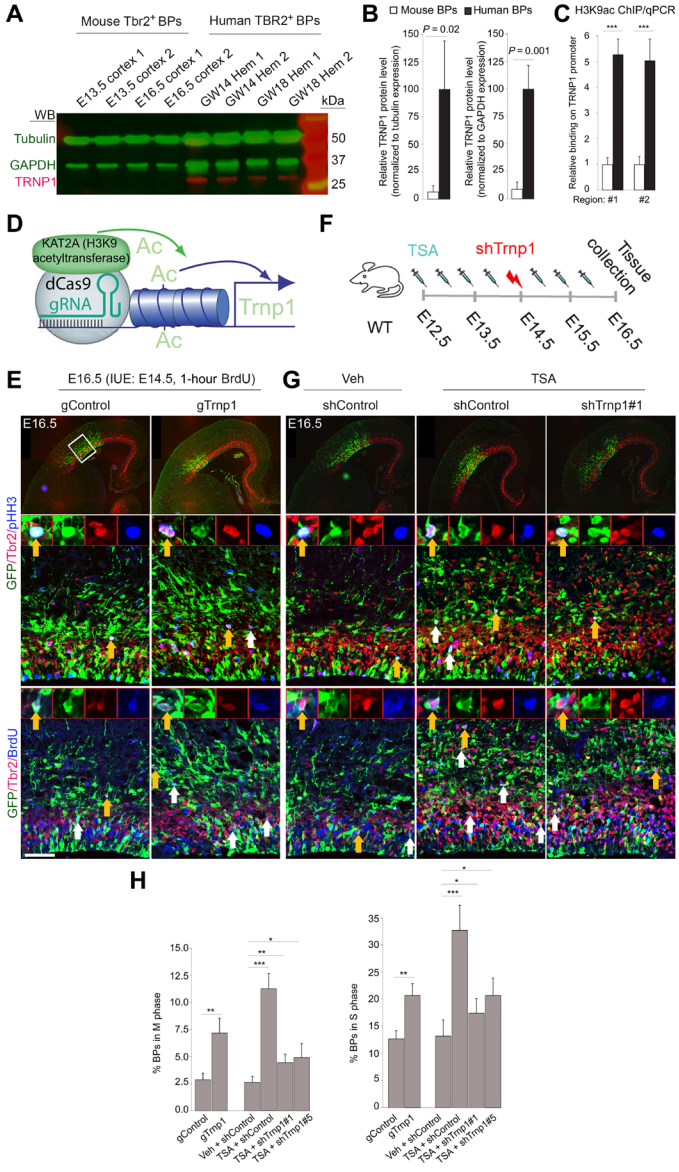


**Fig. 6. H3 acetylation controls the proliferation of bIPs by activating *Trnp1* expression.** (**A** and **B**) WB analysis of protein extracts from Tbr2$^+$ bIPs obtained from mouse and human cortices at the indicated stages, as assessed with antibodies against *Trnp1* (red), tubulin, and GAPDH (green, as loading controls). (B) Relative levels of *Trnp1* protein are presented in the diagram. Little to no *Trnp1* protein is expressed in mouse bIPs, whereas this expression is relatively high in human bIPs. (**C**) ChIP-qPCR comparing the H3K9ac levels at the *Trnp1* promoters in mouse and human Tbr2$^+$ bIPs. (**D**) Schematic overview of the CRISPR-dCas9–based deposition of H3K9ac at the *Trnp1* promoter, which was used to activate its expression. (**E**) Mouse E14.5 d/lCx was in utero electroporated with a g*Trnp1*-dCas9-Kat2a-T2A-eGFP plasmid (g*Trnp1*) or gControl-dCas9-Kat2a-T2A-eGFP plasmid (gControl), and IHC analysis of GFP, Tbr2, pHh3, or 5-bromo-2′-deoxyuridine (BrdU) was performed at E16.5. Images represent triple optical sections. White box indicates areas shown at higher magnification, and red arrows point to examples of cells that are immunoreactive for GFP, Tbr2, pHh3, or BrdU. (**F**) Descriptive scheme of the rescue experiment, in which mouse cortex was treated with the Hdaci, TSA, and g*Trnp1* or shControl constructs at the indicated stages. (**G**) Triple IHC analysis for the markers listed in (E). (**H**) Statistical quantification of the results shown in (E) and (G) is shown. Values are presented as means ± SEM (*$P$ < 0.05, **$P$ < 0.01, and ***$P$ < 0.005). Scale bar, 50 μm.

that *Trnp1* expression was also increased following transfection with the generated editing constructs (fig. S9I). These results validate the ability of the CRISPR-Cas9–mediated epigenome editing system in depositing H3K9ac at the *Trnp1* promoter and increasing the expression of *Trnp1* in neural cells.

To achieve epigenome editing–based modulation of H3K9ac levels in the developing cortex, we delivered the constructs into APs by in utero electroporation (IUE) at E14.5. At E16.5, we analyzed the progeny of the electroporated APs, including $Tbr2^+$ bIPs (Fig. 6, D and E). By comparing the proportion of $Tbr2^+/pHh3^+$ (bIPs in M phase of the cell cycle) and $Tbr2^+$/5-bromo-2′-deoxyuridine $(BrdU)^+$ (bIPs in S phase) cells among the targeted $Tbr2^+$ bIPs (revealed by GFP) in control- and editing construct–injected cortices, we examined whether the altered levels of H3K9ac might influence the proliferation of BPs (Fig. 6, E and H). Similar to TSA treatment, epigenome editing–based augmentation of the promoter H3K9ac level of *Trnp1* increased the percentage of basal mitosis ($GFP^+/Tbr2^+/pHh3^+$ or $BrdU^+$) among targeted bIPs ($GFP^+/Tbr2^+$; Fig. 6, E and H).

Because *Trnp1* overexpression was shown to promote the proliferation of neural stem cells (NSCs) in the developing mouse and ferret cortex (*11*, *22*), we performed rescue expression to examine whether a specific increase in *Trnp1* expression caused the aberrantly enhanced proliferation of bIPs upon TSA treatment. To this end, we electroporated TSA-treated cortex with sh*Trnp1* constructs (*11*) to downregulate *Trnp1* expression (Fig. 6, F and G). The observed TSA treatment–induced proliferation phenotype of $Tbr2^+$ bIPs was largely rescued by *Trnp1* knockdown in the cortex (Fig. 6, G and H). These findings suggest that the elevated level of H3K9ac at the *Trnp1* promoter is directly involved in facilitating the proliferation of $Tbr2^+$ bIPs (also see the model in Fig. 7I).

### Elevated H3ac leads to radial expansion and induces gyrification of the developing mouse cortex

To address the role of H3 acetylation in late corticogenesis in vivo, we treated mouse embryos with TSA for a prolonged period. TSA-treated mice exhibited cortices with larger surface areas compared with Veh-injected controls (Fig. 7, A and B). To evaluate the effect of the increased level of H3 acetylation on neuron production in the developing cortex, we examined the expression of laminar and neuronal subtype-specific genes at E17.5 (Fig. 7C). Immunostaining for the pan-neuronal marker, Neuronal nuclei (NeuN), indicated that there was a considerable increase in cortical radial thickness after TSA treatment (Fig. 7D). The number of Special AT-Rich Sequence-Binding Protein 2 ($Satb2^+$) callosal and $Ctip2^+$ subcerebral projection neurons was also demonstrably increased in the cortex of TSA-treated embryos compared with controls (Fig. 7, E and F).

Previous evidence suggested that an increased number of bRG cells offers extra scaffolding for the radial migration of neurons and causes divergence (fanning out) of radial glial processes in gyrated cortices (*2*, *4*, *10*, *11*). RC2 and Nestin immunostaining, which reveal the layout of RG processes, showed that in the TSA-treated cerebral cortex radial fibers spread out divergently when traversing the CP (fig. S10A, white dashed lines). Fanned-out fibers of $Pax6^+$ bRGs were observed by labeling with the lipophilic dye, DiI, which was applied at the pia (Fig. 3D). At E17.5, most early-born neurons (L6 and L5) had completed their migration. Notably, TSA treatment often led to mild folding of the cortex in WT embryos (fig. S10, B to D), but more profound folding in Baf155cKO mutants in distinct cortical areas, as indicated by L6 (Tbr1) and L5 (Ctip2) immunostaining (Fig. 7G and fig. S10, B to D). Although Hdaci-treated mice died soon after birth, increased folding of TSA-treated cortex was observed at all examined stages [E16.5 to postnatal day 0 (P0)] (fig. S10D). Our findings further corroborate the concordance between abundance of BPs and folding feature of the mammalian cortex as the inhibition of Hdac leads to regionally restricted increases in BPs (fig. S3) and cortical folding (fig. S10B) in sections taken from the rostral, middle, and caudal d/lCx, but not the mCx. We distinguished cortical folding by basement membrane intactness (fig. S10, E and F) and rostro-caudal continuity of both sulci and gyri; this allowed us to distinguish our findings from the defining features of classical neuronal ectopias, such as that seen in lissencephaly type II (also called cobblestone lissencephaly).

Kat2a and kat2b are H3K9 acetyltransferases as the dual deletion of Kat2a and kat2b led to the complete elimination of H3K9ac (*34*, *37*). Because the loss of Kat2a in NSC-specific mouse mutants caused microcephaly (*38*) and Kat2a directly involved in H3K9ac at *Trnp1* promoter (Fig. 6, D and E, and fig. S9, G to I), we investigated whether increasing the level of H3K9ac by overexpressing Kat2a might induce proliferation of BPs and cortical folding. E13.5 WT or *Baf155cKO* brains were electroporated with a *Kat2a*-expression plasmid. Compared with control (GFP-injected cortex) at E15.5, overexpression of *Kat2a* increased the percentage of proliferating BPs ($GFP^+/Ki67^+/Tbr2^+$ or $Pax6^+$) among targeted BPs ($GFP^+/Tbr2^+$ or $Pax6^+$) in WT (fig. S10G) and Baf155cKO cortex (fig. S10H). Furthermore, five of six Baf155cKO and three of six WT cortices injected with *Kat2a* expression plasmids at E12.5 displayed focal neocortex folding at E17.5 (Fig. 7H). Collectively, these findings suggest that increased H3 acetylation at the promoter region of the evolution-related gene, *Trnp1*, selectively promotes the proliferative capacity of bIPs, leading to enhanced neuronal output, increased cortical expansion, and gyrification during mammalian evolution (Fig. 7I).

## DISCUSSION

In this study, we describe H3 acetylation as a previously unknown epigenetic mechanism that regulates neocortical expansion. We present evidence that human BPs have higher H3 acetylation levels than mouse BPs, and that elevated levels of H3ac preferentially promote bIP self-amplification and augment neuronal output, leading to enlarged size and folding of the mouse neocortex (summarized in Fig. 7I). Mechanistically, this process involves the epigenetic and gene expression controls of the evolutionarily regulated gene, *Trnp1*, in cortical development.

### Contribution of BP proliferation to cortical expansion and folding

In lissencephalic rodents, APs in the VZ and $Tbr2^+$ bIPs in the SVZ are largely responsible for neuron production during cortical development. Previous works showed that β-catenin overexpression–induced VZ progenitor amplification in the mouse brain yielded folding of the ventricular surface, not the cortical surface (*39*), and that increasing the pool of BPs/bIPs enlarged the brain size but did not induce cortical folding (*10*, *40*).

On the other hand, published evidence suggests that there is a link between the proportion of BPs/bRGs and the extent of cortical gyrification in various species (*26*, *29*, *41*, *42*). bRG progenitors are derivatives of APs presumably after becoming delaminated from

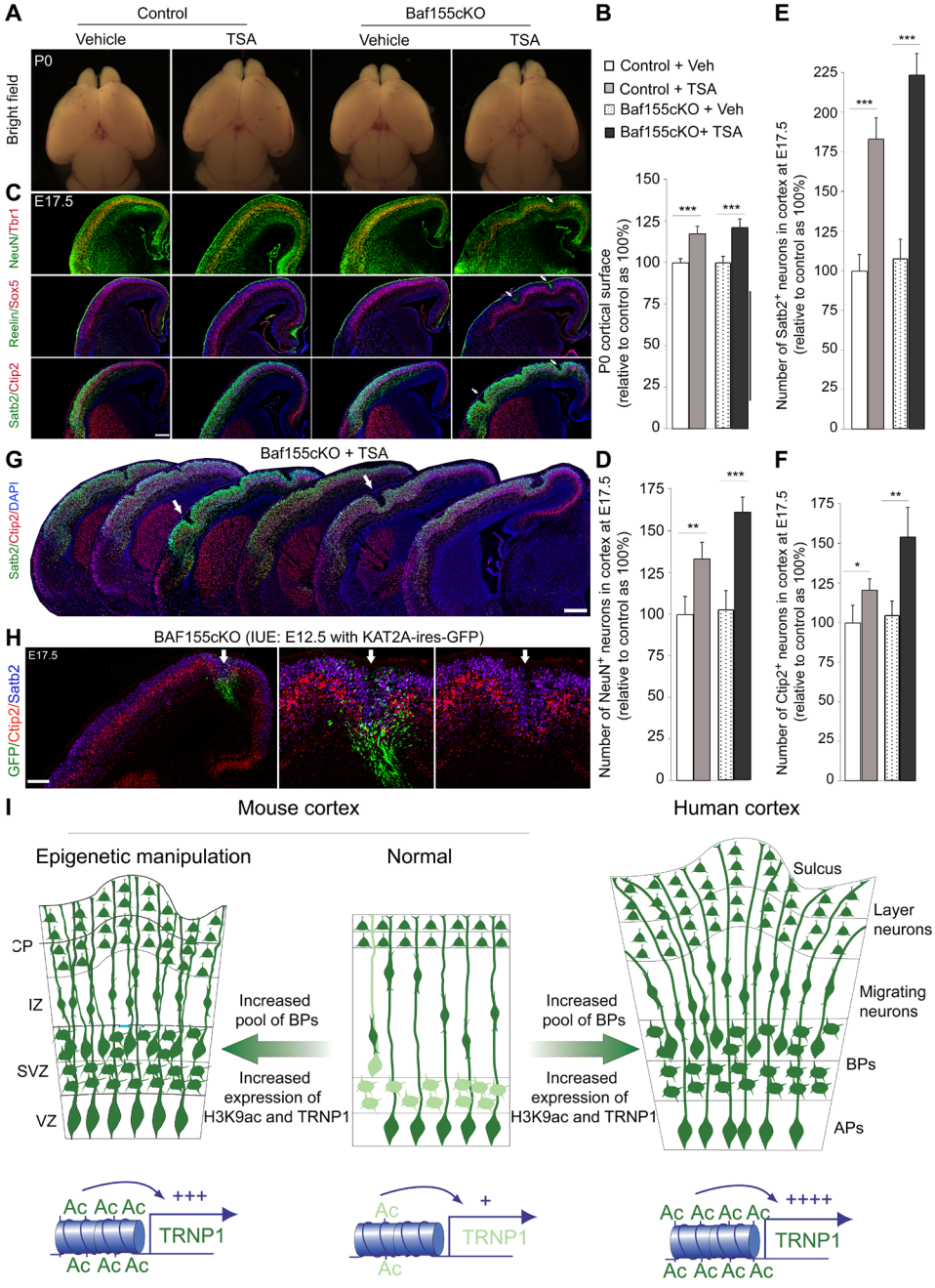


**Fig. 7. Elevated H3ac levels promote cortical expansion and folding.** (**A**) Dorsal-view images of brains from control and Baf155cKO mice with and without TSA treatment (**B**) and quantification of their cortical surfaces at postnatal day 0 (P0) (C) (see also the Supplementary Materials). (**C** to **F**) IHC (C) and quantitation (D to F) of the number of neuronal subsets labeled by the neuronal markers, Satb2, Ctip2, Tbr1, and NeuN, in control and Baf155cKO cortices with and without Hdaci treatment at E17.5. Elevated H3 acetylation increases neurogenesis and cortical thickness and induces gyrification (indicated by arrows). (**G**) Serial coronal sections at E17.5 marked by Ctip2 and Satb2 expression showing the folded cortex in different cortical areas. (**H**) Images of GFP, Satb2, and Ctip2 immunofluorescence of a coronal section of an E17.5 cortical hemisphere from a mouse embryo that had been in utero electroporated at E12.5 with Kat2a-ires-eGFP expression plasmids. Lower images show higher-power magnification of a sulcus-like structure, which is indicated by white arrows. (**I**) Hypothetical model proposing how the changes in H3K9ac levels in evolution and in mouse models with epigenetic manipulation affect the H3K9ac level at the *Trnp1* promoter, the expression of *Trnp1*, the proliferation of BPs, and the expansion and folding of the cortex. +, +++, and ++++ indicate weak, moderate, and strong relative expression levels, respectively (photo credit: Dr. Tran Tuoc, Ruhr University of Bochum). Ac, H3K9ac. Values are presented as means ± SEM (*$P < 0.05$, **$P < 0.01$, and ***$P < 0.005$). Scale bars, 100 μm.

their apical anchorage (*4*). However, when adherens junction proteins are lost (*32*) or the linkages to cytoskeletal belts are broken by down-regulation of the small guanosine triphosphatase, i.e., RhoA, apically anchored progenitor cells are delaminated without notable change in bRG generation or cortical folding. Likewise, our data and that of others indicate that Pax6 and Baf155 control the delamination of RGs at least partly by regulating the expressional programs of genes encoding adherens junction proteins and RhoA

(*32*). Similar to many other mouse mutants that exhibit delamination of APs during corticogenesis, Baf155cKO (*32*, *43*) and Pax6cKO mice (*40*, *44*) do not exhibit an enlarged and folded cortex, suggesting that the ectopic (outside of the VZ) localization of RGs may be insufficient to trigger cortical expansion and/or folding. Recent observations in the cortex of marmoset (a lissencephalic species) or agouti (a rodent with a moderately gyrencephalic cortex) revealed that the presence of an augmented population of bRGs in the expanded oSVZ of some mammalian subclasses may not correlate with the occurrence of cortical folding and gyrencephaly (*45*, *46*). In gyrencephalic ferrets, for example, the oSVZ initially appears as a massing of numerous bRGs that are directly produced by the transient delamination of APs during early cortical development (*22*). Later, however, the generation of bRGs becomes completely independent of AP delamination, instead relying on their self-expansion (*22*). Along the same lines, functional blockade of Tbr2 in ferrets was shown to cause premature neuronal differentiation of SVZ progenitors, diminishing the numbers of bIPs and bRGs and impairing gyrification (*47*). These findings support the idea that BP proliferation is a key driver of cortical folding (*47*). Thus, the simple delamination of VZ progenitors is insufficient to generate BPs with a high proliferative capacity; instead, this process seems to critically involve altered expression of regulatory factors that boost BP amplification.

**H3 acetylation promotes bIP proliferation and cortical expansion**

BPs from rodents and primates have distinct characteristics. In the lissencephalic rodent cortex, BPs are mainly neurogenic progenitors that express the transcription factor (TF), Tbr2. In gyrencephalic species (such as ferret, primate, and human), in contrast, most of the BPs are proliferative progenitors and almost half of them coexpress the TFs, Tbr2 and Pax6 (*2*). In the developing ferret cortex, Tbr2 is essential for the generation of both types of BPs (bIPs and bRGs) (*47*). A prerequisite for identifying the gene expression and epigenetic programs of BPs during evolution is thus the analysis of BP-specific signatures in distinct species. Recent single-cell transcriptomic and genetic studies have sought to elucidate the phylogenic expansion and gyrification of the mammalian cortex (*12*–*14*, *33*, *48*–*50*). A few factors (such as *Trnp1*, *ARHGAP11B*, and *TBC1D3*) have been found to control BP genesis, BP proliferation, cortical expansion, and folding (*10*, *11*, *13*, *15*–*18*, *40*). Recently, remodeling of chromatin via histone PTMs has also been implicated in cortical neurogenesis. However, the epigenetic mechanisms that coordinate the expression or repression of genes that are essential for the developmental events underlying cortical expansion and folding during evolution are still largely unknown.

In this study, we purified Tbr2$^+$ bIPs from mouse and human cortices. To compare the bulk level of epigenetic marks between mouse and human BPs, we quantified the PTMs of histones by simultaneously measuring the relative abundance of most known histone methylation and acetylation marks. This method requires a moderate number of cells that can be obtained by FACS and allows for the systematic screening of epigenetic changes during evolution. We identified a few epigenetic marks that display different levels in Tbr2$^+$ bIPs isolated from mouse versus human cortex. Given that Pax6$^+$ and Sox2$^+$ BPs/bRGs are relatively rare in the WT mouse cortex (*26*, *27*), we used the Baf155cKO mutant as a mouse model to investigate the effect of Hdac inhibition on the proliferation of BPs. On the basis of the expression of Pax6, Ap2γ, and Sox2 in the VZ and pHh3 at the apical VZ surface (Fig. 4, A and C), our data suggest that the elevation of H3ac in developing mouse cortex did not influence the proliferation and delamination of APs, which are consistent with a relatively high basal level of H3K9ac in both mouse and human APs. We found that the level of H3K9ac is higher in human BPs than in mouse BPs. Moreover, we found that elevated H3K9ac specifically expands the pool of BPs, but not APs, and increases the number of both lower-layer Ctip2$^+$ neurons and upper-layer Satb2$^+$ neurons. Our findings revealed that TSA treatment promotes proliferation of Pax6$^+$ BPs and Tbr2$^+$ bIPs. Given that Pax6 labels both bRGs and BPs in transition between bRGs-bIPs in iSVZ/oSVZ, it is still not clear whether increased H3 acetylation boosts the bRG proliferation. As BP population is very heterogeneous (*3*), it is interesting for future studies to examine the effect of H3 acetylation on proliferation of different BP subtypes.

Cortical gyrification is underlined by the production of a large population of neurons and the presence of sufficient and more complex neuronal migration scaffolds, which permit lateral dispersion of neurons to form intricate cortical layers. In gyrencephalic species, cortical expansion is achieved by an extraordinary increase in neurogenic bIPs and the neurogenic/scaffold-forming bRGs in the oSVZ, which are vital in directing lateral dispersion of radially migrating neurons (*1*–*4*). The generation of more bIPs and bRGs in TSA-treated Baf155cKO cortex than in TSA-treated WT cortex could explain the corresponding differences in cortical size (Fig. 7, A to F) and level of cortical folding (fig. S10B) between these two groups. In agreement with previous studies (*19*, *45*, *46*), our findings suggest that the formation of cortical folding requires a great abundance of both bIPs and bRGs.

Cortical folding can be orchestrated by several genes known to critically regulate neuronal migration (*6*). For instance, the cell-adhesion molecules Fibronectin Leucine Rich Transmembrane Protein 1/3 (FLRT1/3) are crucial in modulating cortical neuron radial migration, such that their deficiency caused cortical folds in mouse (*17*). In humans, defective REELIN signaling caused by mutations severely impaired cortical folding (*51*). In TSA-treated cortex (Fig. 7), the sulci correspond to ectopic Reelin$^+$ cells (Fig. 7C). These ectopic Cajal-Retzius neurons could promote aberrant trajectories of RG cells and abnormal migration of neurons. Although our findings highlight a previously unknown epigenetic mechanism underlying cortical folding possibly via increased proliferation of BPs, we do not exclude the possibility that H3 acetylation induces gyrification partly by atypical migration of neurons.

Notably, Hdac inhibition did not activate the expression of known human bRG genes such as Family With Sequence Similarity 107 Member A (FAM107A). Our gene expression comparison revealed that TSA-treated mouse BPs have closer molecular identity with macaque BPs than with those from human. In addition, an increased number of BP cells upon TSA treatment are not observed in the mCx. Apart from H3K9ac, the levels of several other epigenetic marks appeared to be higher in human BPs at GW14 and GW18 than in mouse BPs at E13.5 and E16.5 (Fig. 1D), including H3K18ac, H3K4ac, and H3K4me2, which were also previously shown to be enriched at promoters and enhancers and to activate transcription. These findings suggest that the high proliferative capacity of BPs in mCx and gene expression program of BPs requires high levels of several other epigenetic marks and not on H3K9ac exclusively. Our ongoing work aims to examine whether increased H3K4me2 in cooperative action with H3K9ac could promote expression of BP genes and is able to induce proliferation of BPs in mCx.

Our GO analysis revealed a relatively high expression of genes coding for Hdacs (such as Hdac1, Hdac2, Hdac3, Hdac8, and Hdac9; fig. S2, F to H) in Tbr2$^+$ bIPs in mice. This could explain why levels of H3ac are low in mouse BPs. It will therefore be particularly interesting in the future to investigate the upstream mechanisms and analyze how differential H3 acetylation across different species is modulated. Together, our findings indicate that H3 acetylation has prominent impacts on the cerebral cortex, in terms of both radial and tangential expansion (Fig. 7I), by increasing the population of highly proliferative bIPs and thus the degree of cortical gyrification (as seen in the primate brain).

### *Trnp1* is a main target gene of H3 acetylation in bIP amplification

Our RNA-seq and H3K9ac ChIP-seq analyses for many genes in the sorted Tbr2$^+$ bIPs indicate that Hdac inhibition either increases the H3K9ac level or up-regulates the expression of the studied genes. The correlation of these data indicates that H3K9ac directly activates the expression of only a few genes (Fig. 5, C to H). These genes include *Trnp1*, whose manipulated expression in the mouse and ferret cerebral cortex was previously reported to affect various cortical expansion–related features, including the proliferation of cortical neuroprogenitors and the induction of cortical folding (*11*, *22*, *52*). We herein show that H3K9ac positively regulates the expression of *Trnp1* in bIPs to orchestrate bIP proliferation in the developing cortex. Expressional analyses indicate that the expression patterns of H3K9ac (this study) and *Trnp1* (*11*) are similar in developing mouse and human cortex. In particular, H3K9ac and *Trnp1* exhibit low or undetectable levels in mouse bIPs, whereas their expression is much higher in human bIPs. Furthermore, we show that the overexpression of *Trnp1* by means of H3K9ac epigenome editing increases bIP proliferation, as also seen in Hdaci-treated cortex, and that this phenotype is largely reverted to control levels upon *Trnp1* knockdown. These findings bring to light the role of H3 acetylation as a mechanism upstream of *Trnp1* function for bIP proliferation in cortical development during evolution.

In our observation, the expression of H3K9ac-direct targets such as *Adrb1*, *Trnp1*, and *Pcdh1* is very sensitive and relatively proportional to the level of H3K9ac at their promoters. The TSA treatment led to about 1.5- to 2.3-fold increase in H3K9ac level at the promoter region and about 2.6- to 4.0-fold increase in expression of these genes (Fig. 5, D and H). In the same line of evidence, the treatment of g*Trnp1*#2 increased 1.20-fold in H3K9ac level at its promoter and 1.23-fold in its expression level (fig. S9, H and I). The moderately increased level of H3K9ac at the promoter and expression of key proliferative factor *Trnp1* (*11*, *22*) by the g*Trnp1* electroporation is sufficient to evoke the proliferation of Tbr2$^+$ bIPs in developing mouse cortex (Fig. 6, D, E, and H). Our findings also suggest that the increased expression of many genes upon TSA treatment might synthetically promote the proliferation of BPs. It is worth determining in further studies the function of *Adrb1* and *Pcdh1* alone or together with *Trnp1* in BP amplification and cortical expansion.

In summary, we herein identify a mechanism whereby BP amplification is epigenetically controlled through H3 acetylation, which specifically affects the expression level of *Trnp1*. Our findings show that the temporally dynamic regulation of H3 acetylation and its downstream effector, *Trnp1*, is part of an evolutionary epigenetic mechanism aimed at enlarging the diversity of neocortical phenotypes during evolution.

## MATERIALS AND METHODS

### Plasmids

Plasmids used in this study are as follows: pCIG2-Kat2a-ires-eGFP, g*Trnp1*-dCas9-Kat2a-T2A-eGFP (this study), and sh*Trnp1* constructs (*11*).

### Antibodies

The following polyclonal (pAb) and monoclonal (mAb) primary antibodies used in this study were obtained from the indicated commercial sources: H3K9Ac rabbit pAb (Abcam), Sox2 mouse mAb (1:100; R&D Systems), Sox2 goat (1:100; Santa Cruz Biotechnology), Pax6 mouse mAb (1:100; Developmental Studies Hybridoma Bank), Pax6 rabbit pAb (1:200; Covance), Tbr2 rabbit pAb (1:200; Abcam), Cidu rat pAb (1:100; Accurate), Ki67 rabbit pAb (1:50; Vector Laboratories), GFP rabbit pAb (1:1000; Abcam), GFP chick pAb (1:1000; Abcam), Ap2γ mouse mAb (1:100; Abcam), phospho-H3 rat pAb (1:300; Abcam), pVim mouse mAb (1:500; MBL), Tnc rabbit pAb (Abcam), Ptprz1 rabbit pAb (Sigma-Aldrich), Baf155 rabbit pAb (1:20; Santa Cruz Biotechnology), Baf155 mouse mAb (1:100; Santa Cruz Biotechnology), Casp3 rabbit pAb (1:100; Cell Signaling Technology), Ctip2 rat pAb (1:200; Abcam), HuCD mouse mAb (1:20; Invitrogen), Tbr1 rabbit pAb (1:300; Chemicon), Satb2 mouse mAb (1:200; Abcam), Cux1 rabbit pAb (1:100; Santa Cruz Biotechnology), β-actin rabbit pAb (Sigma-Aldrich), H3ac rabbit pAb (Upstate), NeuN mouse mAb (Chemicon), Reelin mouse mAb (gift from A. Goffine), Sox5 rabbit pAb (Santa Cruz Biotechnology), Kat2a rabbit pAb (Abcam), Nestin mouse mAb (BD), Rc2 mouse mAb (Developmental Studies Hybridoma Bank), Hopx mouse mAb (Santa Cruz Biotechnology, sc-398703), and Hopx rabbit mAb (Sigma-Aldrich, HPA030180).

Secondary antibodies used were horseradish peroxidase (HRP)–conjugated goat anti-rabbit immunoglobulin G (IgG) (1:10,000; Covance), HRP-conjugated goat anti-mouse IgG (1:5000; Covance), HRP-conjugated goat anti-rat IgG (1:10,000; Covance), and Alexa Fluor 488–, Alexa Fluor 568–, Alexa Fluor 594–, and Alexa Fluor 647–conjugated IgG (various species, 1:400; Molecular Probes).

### Human fetal brain collection and processing

Human fetal brain tissue was obtained from spontaneous abortions that occurred in the Hospital for Obstetrics and Gynecology "Prof. Dimitar Stamatov," Medical University of Varna, Bulgaria, after an informed written maternal consent and with the approval of the local ethics committee (protocol no. 19/April 2012; protocol no. 55/June 2016) according to Institutional Review Board guidelines. The gestation age in weeks (GW) has been determined on the basis of the history of last menstruation as reported by the patients. The heads were placed in 4% paraformaldehyde (PFA) solution in phosphate-buffered saline (PBS) (pH 7.5) for 24 hours, and then the brains were dissected and postfixed in PFA for 5 to 7 days, cryoprotected in sucrose, and frozen in optimal cutting temperature medium before cryosectioning at 20 μm. Cortical tissues from additional cases were used for FACS as described for mouse tissues in the below section.

### Animal care, generation of transgenic mice, and IUE

Floxed Baf155 (*53*) and Emx1-Cre (*54*) mice were maintained in a C57BL6/J background. IUE was performed as described previously (*43*, *55*). Animals were handled in accordance with the German Animal Protection Law and with the permission of the Bezirksregierung

Braunschweig according to Institutional Animal Care and Use Committee guidelines.

### Mouse treatment with HDAC inhibitors

TSA (Sigma-Aldrich, catalog no. T8552-1MG) was dissolved in Veh (8% ethanol in 1× PBS) at a concentration of 100 μg/ml. SAHA (Biomol, catalog no. CAS 149647-78-9) was dissolved in Veh [dimethyl sulfoxide (DMSO)] (10 mg/ml). Sodium salt VPA (Sigma-Aldrich, catalog no. P4543) was dissolved in Veh (saline) at concentration of 100 mg/ml. Pregnant mice from E12.5 d.p.c. were injected intraperitoneally twice daily [except the experiment to examine a dose-dependent effect in fig. S4 (A and B)] with either Veh or 150 μl of TSA solution (100 μg/ml) or 20 μl of SAHA solution (10 mg/ml) plus 110 μl of saline or 120 μl of VPA solution (100 mg/ml). Treated mice were euthanized at different developmental stages as indicated in the main text.

### Tbr2$^+$ nuclei and cell sorting from embryonic cortex

Since typical cell sorting methods comprise protease treatment for cell dissociation that can lead to unwanted effects on gene expression profile, we opted for unbiased approach to minimizing biasness due to sample processing. In this regard, we opted for Tbr2$^+$ nuclei sorting from fresh mouse cortex, instead of cell sorting, as this is a well-established method of getting the cell types of interest from the brain without the biasness of the sample preparation (*23*, *24*). Since we were interested to obtain epigenetic and transcriptomic data from Tbr2$^+$ and Tbr2$^-$ nuclei, two different protocols were followed, respectively. By unknown reasons, Tbr2 antibody did not work in our intracellular immunostaining protocols for nuclei, which were prepared from frozen tissue.

In our MS analysis, we used frozen human cortex as the cell source for sorting. We therefore establish a cell preparation protocol using solution with stringent reagents for cell sorting.

#### *Tbr2$^+$ nuclei sorting protocol from embryonic mouse brain for ChIP-seq*

The protocol was adapted originally from a previously published protocol (*23*, *24*). All steps were performed on ice or at 4° unless stated otherwise. Freshly prepared embryonic cortices from five CD1 pups were pooled for each replicates and homogenized briefly in low-sucrose buffer [320 mM sucrose, 5 mM $CaCl_2$, 5 mM $MgAc_2$, 0.1 mM EDTA, 10 mM Hepes (pH 8), 0.1% Triton X-100, and 1 mM dithiothreitol (DTT), supplemented with Roche protease inhibitor cocktail] with plastic pestles in 1.5-ml tubes. Cross-linking was performed with 1% formaldehyde and incubated for 10 min at room temperature on a rotating wheel. Glycine (125 mM) was used for quenching remaining formaldehyde in solution by incubation for 5 min at room temperature. After centrifugation at 2000*g* for 3 min, the crude nuclear pellet was pipetted, mixed into additional low-sucrose buffer, and further homogenized with a mechanical homogenizer (IKA ULTRA-TURRAX). The solution was carefully layered on high-sucrose buffer [1000 mM sucrose, 3 mM magnesium acetate, 10 mM Hepes (pH 8), 1 mM DTT, and protease inhibitor] in oak-ridge tubes and spinned at 3200*g* for 10 min in a swinging bucket rotor centrifuge. This was performed to get rid of myelin. Supernatant was carefully removed without disturbing the nuclear pellet and transferred into 2-ml microfuge tubes (DNA low bind). Nuclei were collected by centrifuging for 3 min at 2000*g*. After removing remaining sucrose buffer, nuclei were resuspended into 500 μl of PBTB buffer [PBS 0.2%–Tween 1%–bovine serum albumin (BSA) buffer, with protease inhibitor]. Tbr2 staining was performed using anti-Tbr2 (Eomes) Alexa Fluor 488–conjugated antibody (1:100; IC8889G-025) for 1 hour. Nuclei were washed once and lastly resuspened into 500 μl of PBTB. FACSAria III was used to performing Tbr2 nuclei sorting, while samples without antibody acted as negative control for gating. Nuclei were sorted directly into PBTB-coated 15-ml falcon tubes and centrifuged briefly to pellet the Tbr2 positive and negative nuclei. Sorted nuclei pellets were flash-frozen into liquid nitrogen and stored at −80°C before proceeding with ChIP experiment.

#### *Tbr2$^+$ nuclei sorting protocol from embryonic mouse brain for RNA isolation and RNA-seq*

Freshly dissected mouse embryonic cortices from five CD1 pups were pooled and immediately submerged into enough RNAlater solution in a microfuge tube and kept at 4°C for at least 24 hours. The excess RNAlater solution were pipetted out and washed twice with 1× ribonuclease (RNAse)–free PBS. After last wash, all the incubation steps were performed on ice or centrifugation at 500*g* at 4° unless stated otherwise. The tissues were immediately submerged into 500 μl of lysis buffer (Sigma-Aldrich, NUC101) and dounce-homogenized using plastic pestles for 30 to 45 times, and additional lysis buffer was added to make the volume up to 2 ml. After incubating for 7 min, lysates were centrifuged for 5 min, and nuclei pellet was resuspended into 2 ml of lysis buffer. Lysates were incubated for 7 min, filtered through 40-μm filter into a new 2-ml tube, and centrifuged to remove supernatant. Pellet was washed with 1800 μl of nuclei suspension buffer [NSB; 0.5% RNAse-free BSA (Millipore), 1:200 RNaseIN plus RNAse inhibitor (Promega), protease inhibitor diluted into RNAse-free PBS (Invitrogen)] by centrifuging and resuspended in 500 μl of NSB. Tbr2 staining was performed using anti-Tbr2 (Eomes) Alexa Fluor 488–conjugated antibody (1:100; IC8889G-025) for 1 hour. Stained nuclei were washed and resuspended both using NSB. Nuclei sorting were performed in the aforementioned section (Tbr2 nuclei sorting for ChIPseq), while sorted nuclei were collected into NSB-coated falcon tubes. Nuclei were collected with brief centrifugation, and TRIzol LS solution was added for RNA isolation. After adding chloroform and centrifugation for 15 min at 120,000*g*, aqueous phase was collected, and RNA was purified with Zymo RNA Clean & Concentrator-5 kit. Resulting RNA was used with Takara SMART-Seq v4 Ultra Low Input RNA kit to prepare mRNA-seq libraries using 1 ng of RNA from sorted Tbr2 nuclei. Libraries were sequenced in Illumina Hiseq 2000 machine.

#### *Tbr2$^+$ cell sorting protocol from embryonic mouse brain for MS analysis*

We pooled at least eight (at E13.5) or four (E16.5) mouse cortices or equal amount of human cortex per replicate. Cortical cells were dissociated using the neural tissue dissociation kit (MACS Miltenyi Biotec, #130-092-628P). Subsequently, cells were fixed and permeabilized with the Foxp3 Fixation/Permeabilization working solution (Foxp3/Transcription Factor Staining Buffer Set, eBioscience, #00-5523). For antibody labeling, cells were incubated with Alexa Fluor 488–conjugated Tbr2 antibody (1:200 in permeabilization buffer) for at least 30 min on ice (in the dark) with slight shaking. Stained cells then were washed twice with permeabilization buffer. After sorting, pellet of the sorted cells was collected by centrifugation. Samples should be stored in −80°C if the experiment is not performed immediately.

### MS analysis of epigenetic marks

Histones were prepared from 2.5 × $10^6$ sorted Tbr2$^+$ cells for each MS sample. Histone extraction and MS analysis were performed as

described previously (*56*). To generate the heatmaps, for each individual modification, the data for each sample were converted to the fraction of the sum across all samples to display relative abundances across the sample group and then conditionally formatted in Excel using the default red/white/blue color scheme. The hierarchical clustering heatmap was generated in R using the "pheatmap" function with default settings.

### Chromatin immunoprecipitation

The ChIP protocol was described previously (*57*) with H3K9ac antibody (Millipore, 07-352). Resulting ChIPed DNA was used for either qPCR or sequencing for appropriate experiments. For ChIP sequencing, immunoprecipitated DNA was further processed with NEBNext Ultra II DNA library preparation kit to generate Illumina sequencing libraries. Libraries were sequenced in Illumina Hiseq 2000 machine.

### Next-generation sequencing data analysis (ChIP-seq and RNA-seq)

Base calling and conversion to fastq format were performed using Illumina pipeline scripts. Afterward, quality control on raw data was conducted for each library (FastQC, www.bioinformatics.babraham.ac.uk/projects/fastqc). The following control measurements and information were obtained: per base sequence quality, per sequence quality scores, per base sequence content, per base guanine-cytosine (GC) content, per sequence GC content, per base N content, sequence length distribution, sequence duplication levels, overrepresented sequences, and Kmer content. The reads were mapped to a mouse reference genome (mm10) using bowtie2. and *rmdup* function of SAMTools (*58*) was used to remove PCR duplicates from each BAM file. *merge* function of SAMTools was used for merging BAM files with unique reads (i.e., with duplicates removed) belonging to replicates from the same group into a single BAM file. All the downstream analyses were performed on BAM files with only unique reads. Profile plots of H3K9ac were created with NGSPlot using merged BAM files from immunoprecipitated samples and inputs. H3K9ac enrichment at different gene loci was visualized through the Integrated Genome Browser using wiggle files that were created from the merged BAM files with the script from the MEDIPS package of Bioconductor. Peaks were called on individual with MACS2 with $q < 0.1$. Differential binding was assessed with DiffBind package of Bioconductor with in-built DESEQ2 option implemented in differential analysis. In differential binding analyses, promoters were defined as ±2000 base pairs (bp) from transcription start site. Peak annotation was performed with HOMER. RNA-seq was performed as described previously (*57*, *59*).

### Epigenome editing

#### *Constructs for epigenome editing*

The backbone vector encoding single gRNAs (sgRNAs) and 3xFlag–dCas9 (nuclease dead Cas9)–T2A-GFP expression cassette was generated from the vector pSpCas9n(BB)-2A-GFP (PX461 in Addgene): H840A was introduced into Cas9n to produce dCas9 through PCR-mediated mutagenesis cloning, and a polylinker sequence 5′-TCCGGACGGGGATCCACTAGTGTCGACACCGGTCCTAGG-3′ was inserted right after the Cas9 coding sequence. The vectors for the mouse *Trnp1* promoter epigenome editing were derived from the above generated backbone vector. gRNA sequences targeting specific mouse *Trnp1* promoter region (Chr4: 133497514 to 133498529) was designed using the software "Geneious" and cloned into the vector between Bbs I sites after in vitro test, and then the coding sequence for mouse Kat2a was amplified from the vector pCMV-sport2-mGcn5 (gift from S. Dent, Addgene plasmid #23098) and cloned into the backbone vector between Spe I and Avr II sites, in frame with that of dsCas9 and T2A-GFP. The vectors were confirmed by sequencing.

### In vitro test for Trnp1 sgRNAs, quantification of H3K9ac level at Trnp1 promoter, and expression of Trnp1 in gTrnp1-dCas9-Kat2a–transfected Neuro2A

For in vitro test, sgRNAs were synthesized through in vitro transcription from a PCR-produced sgRNA template, which harbors the T7 promoter abided by the gRNA sequence and the sharped gRNA scaffold using MEGAscript T7 Transcription Kit (Invitrogen) according to the manufacturer's protocols. Cas9 protein was purchased from IDT (#1074182). In vitro test of Cas9/gRNA complexes cutting efficiency was performed using a 1016-bp PCR product from *Trnp1* promoter according the protocol described in (*36*).

On the basis of the in vitro testing result, the gRNA2 and gRNA4 were selected and cloned into above mentioned vector to generate vectors *Trnp1*-sg2-Flag-dCas9-2A-GFP (*Trnp1*-sg2) and *Trnp1*-sg4-Flag-dCas9-2A-GFP (*Trnp1*-sg4). Twelve micrograms of parental vector Flag-dCas9-2A-GFP or *Trnp1*-sg2 or/and *Trnp1*-sg4 were transfected into Neuro2A cells cultured on 10-cm dishes using Lipofectamine 2000 reagent (Thermo Fisher Scientific) following the manufacturer's protocol, and cells were harvested for FACS analysis 3 days after transfection for qPCR and ChIP/qPCR analyses.

### Cell cultures

For cell culture assays, plasmids were transfected into Neuro2A cells using Lipofectamine 2000 or were electroporated into primary cortical cells using a mouse neural cell Nucleofector kit and a nucleotransfection device (Amaxa).

### IHC, cell cycle parameter, and DiI-labeling experiments

IHC, determination of cell cycle index, and DiI labeling were performed as previously described (*36*, *44*). IHC analysis for Hopx was described previously (*27*). Briefly, the antigen retrieval was performed by incubating the brain sections in 0.01 M sodium citrate buffer for 60 min at 70°C, followed by cooldown for 20 min at room temperature. Sections were then permeabilized with 0.3% (w/v) Triton X-100 in PBS for 30 min and quenched with 2 mM glycine in PBS for 30 min, followed by blocking with a solution containing 0.2% (w/v) gelatin, 300 mM NaCl, and 0.3% (w/v) Triton X-100 in PBS (blocking buffer). The Hopx antibody (1:200; Sigma-Aldrich, catalog no. HPA030180) was diluted in blocking buffer and sections incubated with primary antibody at 4°C for 2 days. Incubation with primary antibodies was followed by a 1-hour incubation at room temperature with the appropriate Alexa Fluor 488–, Alexa Fluor 594–, Alexa Fluor 555–, or Alexa Fluor 647–labeled (1:400; Alexa Fluor series, Invitrogen) secondary goat or donkey antibodies.

### Retrovirus production and viral infection in slices

Retrovirus for GFP labeling was produced from 293gp NIT-GFP packaging cells by transfection with pCMV-VSV-G plasmid (Addgene, #8454). Viral particles with low titer of about $10^6$ plaque-forming units (PFU)/ml were used for infection. For the viral infection, cortical slices from the brain of TSA-treated Baf155cKO embryos were prepared and cultured as described previously (*57*). To label the bRGs, GFP-expressing retrovirus (106 PFU/ml) was injected

into IZ of the cultured cortical slice, using a glass micropipette. Sixty hours after infection, brain slides were washed and stained with antibodies against GFP and Pax6.

### Quantitative reverse transcription PCR and WB analyses

Quantitative reverse transcription PCR and WB analyses were performed as described previously (*55*) using primers described in table S7 and the RT$^2$ Profiler PCR Array profiles (QIAGEN).

### Relative quantification of cortical surface, cell counts, and quantitative analysis of IHC signal intensity

The cortical surface was measured and analyzed as described previously (*32*, *40*). For the quantitative analyses of IHC signal intensity of H3K9ac and H3ac, confocal fluorescent images of sections of mouse and human cortex were used. The IHC images with corresponding IgG isotopes were used as immunostaining controls. The color images of cortex were converted to gray scale to eliminate background. The pixel values of the fluorescent signal intensity were measured using Analyze/Analyze Particles function (ImageJ software) as previously described (*40*, *60*). The measured value was then subtracted from immune-staining controls (without primary antibody). Similarly, the relative amount of protein from developed films in WB experiment was quantified densitometrically using ImageJ software as described previously (*40*, *60*).

Immunomicrographs were quantified using anatomically matched forebrain sections from control and mutants or Hdaci-treated embryos. Marker-positive cells within images of the cortex obtained by confocal microscopy were counted for comparison.

In developing mouse cortex, expression level of Pax6 is very variable from Pax6$^{low}$ to Pax6$^{high}$ in cortical progenitors (*55*). In some cells, expression of Pax6 is even at the border between background and very low (Pax6$^{very\ low}$). We noted that TSA treatment massively increased the number of Pax6$^+$ cells in SVZ/IZ. Among these Pax6$^+$ cells, many are Pax6$^{very\ low}$. In our cell counting and quantification for Pax6$^+$ cells, images were acquired with confocal microscopes and were further analyzed with Adobe Photoshop. We adjusted the brightness of images for both TSA- and Veh-treated samples to mask Pax6$^{very\ low}$ cells.

In general, cell counts of six matched sections were averaged from three biological replicates. Student's *t* test was used to statistically analyze histological data. All statistical tests are two-tailed, and *P* values are considered significant for $\alpha = 0.05$. Bar graphs are plotted as means ± SEM. Details of statistical analyses of histological experiments are presented in table S9.

### Image acquisition and statistical analysis

Images were acquired with epifluorescence (Leica DM 6000) and confocal microscopes (Leica TCS SP5). Adobe Photoshop was used to process images for further analyses. Statistical significance was determined by Student's *t* test or Mann-Whitney *U* test. All graphs are plotted as means ± SEM. The statistical quantification was performed as average from at least three biological replicate. All details of statistical analyses for histological experiments are presented in table S9.

## SUPPLEMENTARY MATERIALS

Supplementary material for this article is available at https://science.org/doi/10.1126/sciadv.abc6792

View/request a protocol for this paper from *Bio-protocol*.

## REFERENCES AND NOTES


1. E. Taverna, M. Gotz, W. B. Huttner, The cell biology of neurogenesis: Toward an understanding of the development and evolution of the neocortex. *Annu. Rev. Cell Dev. Biol.* **30**, 465–502 (2014).
2. J. H. Lui, D. V. Hansen, A. R. Kriegstein, Development and evolution of the human neocortex. *Cell* **146**, 18–36 (2011).
3. C. Dehay, H. Kennedy, K. S. Kosik, The outer subventricular zone and primate-specific cortical complexification. *Neuron* **85**, 683–694 (2015).
4. V. Borrell, M. Gotz, Role of radial glial cells in cerebral cortex folding. *Curr. Opin. Neurobiol.* **27**, 39–46 (2014).
5. Z. Molnar, G. J. Clowry, N. Šestan, A. Alzu'bi, T. Bakken, R. F. Hevner, P. S. Hüppi, I. Kostović, P. Rakic, E. S. Anton, D. Edwards, P. Garcez, A. Hoerder-Suabedissen, A. Kriegstein, New insights into the development of the human cerebral cortex. *J. Anat.* **235**, 432–451 (2019).
6. C. Llinares-Benadero, V. Borrell, Deconstructing cortical folding: Genetic, cellular and mechanical determinants. *Nat. Rev. Neurosci.* **20**, 161–176 (2019).
7. R. F. Hevner, Intermediate progenitors and Tbr2 in cortical development. *J. Anat.* **235**, 616–625 (2019).
8. N. A. Vasistha, F. García-Moreno, S. Arora, A. F. P. Cheung, S. J. Arnold, E. J. Robertson, Z. Molnár, Cortical and clonal contribution of Tbr2 expressing progenitors in the developing mouse brain. *Cereb. Cortex* **25**, 3290–3302 (2015).
9. M. Betizeau, V. Cortay, D. Patti, S. Pfister, E. Gautier, A. Bellemin-Ménard, M. Afanassieff, C. Huissoud, R. J. Douglas, H. Kennedy, C. Dehay, Precursor diversity and complexity of lineage relationships in the outer subventricular zone of the primate. *Neuron* **80**, 442–457 (2013).
10. M. Nonaka-Kinoshita, I. Reillo, B. Artegiani, M. Ángeles Martínez-Martínez, M. Nelson, V. Borrell, F. Calegari, Regulation of cerebral cortex size and folding by expansion of basal progenitors. *EMBO J.* **32**, 1817–1828 (2013).
11. R. Stahl, T. Walcher, C. de Juan Romero, G. A. Pilz, S. Cappello, M. Irmler, J. M. Sanz-Aquela, J. Beckers, R. Blum, V. Borrell, M. Götz, Trnp1 regulates expansion and folding of the mammalian cerebral cortex by control of radial glial fate. *Cell* **153**, 535–549 (2013).
12. M. B. Johnson, P. P. Wang, K. D. Atabay, E. A. Murphy, R. N. Doan, J. L. Hecht, C. A. Walsh, Single-cell analysis reveals transcriptional heterogeneity of neural progenitors in human cortex. *Nat. Neurosci.* **18**, 637–646 (2015).
13. M. Florio, M. Albert, E. Taverna, T. Namba, H. Brandl, E. Lewitus, C. Haffner, A. Sykes, F. K. Wong, J. Peters, E. Guhr, S. Klemroth, K. Prufer, J. Kelso, R. Naumann, I. Nusslein, A. Dahl, R. Lachmann, S. Paabo, W. B. Huttner, Human-specific gene ARHGAP11B promotes basal progenitor amplification and neocortex expansion. *Science* **347**, 1465–1470 (2015).
14. A. A. Pollen, T. J. Nowakowski, J. Chen, H. Retallack, C. Sandoval-Espinosa, C. R. Nicholas, J. Shuga, S. J. Liu, M. C. Oldham, A. Diaz, D. A. Lim, A. A. Leyrat, J. A. West, A. R. Kriegstein, Molecular identity of human outer radial glia during cortical development. *Cell* **163**, 55–67 (2015).
15. B. I. Bae, I. Tietjen, K. D. Atabay, G. D. Evrony, M. B. Johnson, E. Asare, P. P. Wang, A. Y. Murayama, K. Im, S. N. Lisgo, L. Overman, N. Sestan, B. S. Chang, A. J. Barkovich, P. E. Grant, M. Topcu, J. Politsky, H. Okano, X. Piao, C. A. Walsh, Evolutionarily dynamic alternative splicing of GPR56 regulates regional cerebral cortical patterning. *Science* **343**, 764–768 (2014).
16. L. Wang, S. Hou, Y. G. Han, Hedgehog signaling promotes basal progenitor expansion and the growth and folding of the neocortex. *Nat. Neurosci.* **19**, 888–896 (2016).
17. D. Del Toro, T. Ruff, E. Cederfjäll, A. Villalba, G. Seyit-Bremer, V. Borrell, R. Klein, Regulation of cerebral cortex folding by controlling neuronal migration via FLRT adhesion molecules. *Cell* **169**, 621–635.e16 (2017).
18. X. C. Ju, Q. Q. Hou, A. L. Sheng, K. Y. Wu, Y. Zhou, Y. Jin, T. Wen, Z. Yang, X. Wang, Z. G. Luo, The hominoid-specific gene TBC1D3 promotes generation of basal neural progenitors and induces cortical folding in mice. *eLife* **5**, e18197 (2016).
19. J. Liu, W. Liu, L. Yang, Q. Wu, H. Zhang, A. Fang, L. Li, X. Xu, L. Sun, J. Zhang, F. Tang, X. Wang, The primate-specific gene *TMEM14B* marks outer radial glia cells and promotes cortical expansion and folding. *Cell Stem Cell* **21**, 635–649.e8 (2017).
20. I. T. Fiddes, G. A. Lodewijk, M. Mooring, C. M. Bosworth, A. D. Ewing, G. L. Mantalas, A. M. Novak, A. van den Bout, A. Bishara, J. L. Rosenkrantz, R. Lorig-Roach, A. R. Field, M. Haeussler, L. Russo, A. Bhaduri, T. J. Nowakowski, A. A. Pollen, M. L. Dougherty, X. Nuttle, M.-C. Addor, S. Zwolinski, S. Katzman, A. Kriegstein, E. E. Eichler, S. R. Salama, F. M. J. Jacobs, D. Haussler, Human-specific *NOTCH2NL* genes affect notch signaling and cortical neurogenesis. *Cell* **173**, 1356–1369.e22 (2018).
21. I. K. Suzuki, D. Gacquer, R. Van Heurck, D. Kumar, M. Wojno, A. Bilheu, A. Herpoel, N. Lambert, J. Cheron, F. Polleux, V. Detours, P. Vanderhaeghen, Human-specific *NOTCH2NL* genes expand cortical neurogenesis through delta/notch regulation. *Cell* **173**, 1370–1384.e16 (2018).
22. M. A. Martínez-Martínez, C. D. J. Romero, V. Fernández, A. Cárdenas, M. Götz, V. Borrell, A restricted period for formation of outer subventricular zone defined by Cdh1 and Trnp1 levels. *Nat. Commun.* **7**, 11812 (2016).

23. P. A. Ulmke, M. S. Sakib, P. Ditte, G. Sokpor, C. Kerimoglu, L. Pham, Y. Xie, X. Mao, J. Rosenbusch, U. Teichmann, H. P. Nguyen, A. Fischer, G. Eichele, J. F. Staiger, T. Tuoc, Molecular profiling reveals involvement of ESCO2 in intermediate progenitor cell maintenance in the developing mouse cortex. *Stem Cell Rep.* **16**, 968–984 (2021).
24. M. S. Sakib, G. Sokpor, H. P. Nguyen, A. Fischer, T. Tuoc, Intranuclear immunostaining-based FACS protocol from embryonic cortical tissue. *STAR Protoc.* **2**, 100318 (2021).
25. C. Englund, A. Fink, C. Lau, D. Pham, R. A. Daza, A. Bulfone, T. Kowalczyk, R. F. Hevner, Pax6, Tbr2, and Tbr1 are expressed sequentially by radial glia, intermediate progenitor cells, and postmitotic neurons in developing neocortex. *J. Neurosci.* **25**, 247–251 (2005).
26. X. Wang, J. W. Tsai, B. LaMonica, A. R. Kriegstein, A new subtype of progenitor cell in the mouse embryonic neocortex. *Nat. Neurosci.* **14**, 555–561 (2011).
27. S. Vaid, J. G. Camp, L. Hersemann, C. E. Oegema, A.-K. Heninger, S. Winkler, H. Brandl, M. Sarov, B. Treutlein, W. B. Huttner, T. Namba, A novel population of Hopx-dependent basal radial glial cells in the developing mouse neocortex. *Development* **145**, dev169276 (2018).
28. S. A. Fietz, I. Kelava, J. Vogt, M. Wilsch-Bräuninger, D. Stenzel, J. L. Fish, D. Corbeil, A. Riehn, W. Distler, R. Nitsch, W. B. Huttner, OSVZ progenitors of human and ferret neocortex are epithelial-like and expand by integrin signaling. *Nat. Neurosci.* **13**, 690–699 (2010).
29. D. V. Hansen, J. H. Lui, P. R. Parker, A. R. Kriegstein, Neurogenic radial glia in the outer subventricular zone of human neocortex. *Nature* **464**, 554–561 (2010).
30. B. Yao, K. M. Christian, C. He, P. Jin, G. L. Ming, H. Song, Epigenetic mechanisms in neurogenesis. *Nat. Rev. Neurosci.* **17**, 537–549 (2016).
31. Y. Hirabayashi, Y. Gotoh, Epigenetic control of neural precursor cell fate during development. *Nat. Rev. Neurosci.* **11**, 377–388 (2010).
32. R. Narayanan, L. Pham, C. Kerimoglu, T. Watanabe, R. C. Hernandez, G. Sokpor, P. A. Ulmke, K. A. Kiszka, A. B. Tonchev, J. Rosenbusch, R. H. Seong, U. Teichmann, J. Frahm, A. Fischer, S. Bonn, A. Stoykova, J. F. Staiger, T. Tuoc, Chromatin remodeling BAF155 subunit regulates the genesis of basal progenitors in developing cortex. *iScience* **4**, 109–126 (2018).
33. Y. Arai, J. N. Pulvers, C. Haffner, B. Schilling, I. Nüsslein, F. Calegari, W. B. Huttner, Neural stem and progenitor cells shorten S-phase on commitment to neuron production. *Nat. Commun.* **2**, 154 (2011).
34. Q. Jin, L. Zhuang, B. Lai, C. Wang, W. Li, B. Dolan, Y. Lu, Z. Wang, K. Zhao, W. Peng, S. Y. R. Dent, K. Ge, Gcn5 and PCAF negatively regulate interferon-β production through HAT-independent inhibition of TBK1. *EMBO Rep.* **15**, 1192–1201 (2014).
35. A. A. Pollen, A. Bhaduri, M. G. Andrews, T. J. Nowakowski, O. S. Meyerson, M. A. Mostajo-Radji, E. D. Lullo, B. Alvarado, M. Bedolli, M. L. Dougherty, I. T. Fiddes, Z. N. Kronenberg, J. Shuga, A. A. Leyrat, J. A. West, M. Bershteyn, C. B. Lowe, B. J. Pavlovic, S. R. Salama, D. Haussler, E. E. Eichler, A. R. Kriegstein, Establishing cerebral organoids as models of human-specific brain evolution. *Cell* **176**, 743–756.e17 (2019).
36. M. Albert, N. Kalebic, M. Florio, N. Lakshmanaperumal, C. Haffner, H. Brandl, I. Henry, W. B. Huttner, Epigenome profiling and editing of neocortical progenitor cells during development. *EMBO J.* **36**, 2642–2658 (2017).
37. J. V. Tjeertes, K. M. Miller, S. P. Jackson, Screen for DNA-damage-responsive histone modifications identifies H3K9Ac and H3K56Ac in human cells. *EMBO J.* **28**, 1878–1889 (2009).
38. V. Martínez-Cerdeño, J. M. Lemen, V. Chan, A. Wey, W. Lin, S. R. Dent, P. S. Knoepfler, N-Myc and GCN5 regulate significantly overlapping transcriptional programs in neural stem cells. *PLOS ONE* **7**, e39456 (2012).
39. A. Chenn, C. A. Walsh, Regulation of cerebral cortical size by control of cell cycle exit in neural precursors. *Science* **297**, 365–369 (2002).
40. T. C. Tuoc, S. Boretius, S. N. Sansom, M. E. Pitulescu, J. Frahm, F. J. Livesey, A. Stoykova, Chromatin regulation by BAF170 controls cerebral cortical size and thickness. *Dev. Cell* **25**, 256–269 (2013).
41. A. Shitamukai, D. Konno, F. Matsuzaki, Oblique radial glial divisions in the developing mouse neocortex induce self-renewing progenitors outside the germinal zone that resemble primate outer subventricular zone progenitors. *J. Neurosci.* **31**, 3683–3695 (2011).
42. I. Reillo, C. de Juan Romero, M. A. Garcia-Cabezas, V. Borrell, A role for intermediate radial glia in the tangential expansion of the mammalian cerebral cortex. *Cereb. Cortex* **21**, 1674–1694 (2011).
43. Y. Xie, R. Castro-Hernández, G. Sokpor, L. Pham, R. Narayanan, J. Rosenbusch, J. F. Staiger, T. Tuoc, RBM15 modulates the function of chromatin remodeling factor BAF155 through RNA methylation in developing cortex. *Mol. Neurobiol.* **56**, 7305–7320 (2019).
44. T. C. Tuoc, K. Radyushkin, A. B. Tonchev, M. C. Pinon, R. Ashery-Padan, Z. Molnar, M. S. Davidoff, A. Stoykova, Selective cortical layering abnormalities and behavioral deficits in cortex-specific Pax6 knock-out mice. *J. Neurosci.* **29**, 8335–8349 (2009).
45. F. Garcia-Moreno, N. A. Vasistha, N. Trevia, J. A. Bourne, Z. Molnar, Compartmentalization of cerebral cortical germinal zones in a lissencephalic primate and gyrencephalic rodent. *Cereb. Cortex* **22**, 482–492 (2012).
46. I. Kelava, I. Reillo, A. Y. Murayama, A. T. Kalinka, D. Stenzel, P. Tomancak, F. Matsuzaki, C. Lebrand, E. Sasaki, J. C. Schwamborn, H. Okano, W. B. Huttner, V. Borrell, Abundant occurrence of basal radial glia in the subventricular zone of embryonic neocortex of a lissencephalic primate, the common marmoset Callithrix jacchus. *Cereb. Cortex* **22**, 469–481 (2012).
47. T. Toda, Y. Shinmyo, T. A. Dinh Duong, K. Masuda, H. Kawasaki, An essential role of SVZ progenitors in cortical folding in gyrencephalic mammals. *Sci. Rep.* **6**, 29578 (2016).
48. C. de Juan Romero, C. Bruder, U. Tomasello, J. M. Sanz-Anquela, V. Borrell, Discrete domains of gene expression in germinal layers distinguish the development of gyrencephaly. *EMBO J.* **34**, 1859–1874 (2015).
49. S. A. Fietz, R. Lachmann, H. Brandl, M. Kircher, N. Samusik, R. Schroder, N. Lakshmanaperumal, I. Henry, J. Vogt, A. Riehn, W. Distler, R. Nitsch, W. Enard, S. Paabo, W. B. Huttner, Transcriptomes of germinal zones of human and mouse fetal neocortex suggest a role of extracellular matrix in progenitor self-renewal. *Proc. Natl. Acad. Sci. U.S.A.* **109**, 11836–11841 (2012).
50. E. R. Thomsen, J. K. Mich, Z. Yao, R. D. Hodge, A. M. Doyle, S. Jang, S. I. Shehata, A. M. Nelson, N. V. Shapovalova, B. P. Levi, S. Ramanathan, Fixed single-cell transcriptomic characterization of human radial glial diversity. *Nat. Methods* **13**, 87–93 (2016).
51. S. E. Hong, Y. Y. Shugart, D. T. Huang, S. A. Shahwan, P. E. Grant, J. O.'. B. Hourihane, N. D. T. Martin, C. A. Walsh, Autosomal recessive lissencephaly with cerebellar hypoplasia is associated with human RELN mutations. *Nat. Genet.* **26**, 93–96 (2000).
52. G. A. Pilz, A. Shitamukai, I. Reillo, E. Pacary, J. Schwausch, R. Stahl, J. Ninkovic, H. J. Snippert, H. Clevers, L. Godinho, F. Guillemot, V. Borrell, F. Matsuzaki, M. Götz, Amplification of progenitors in the mammalian telencephalon includes a new radial glial cell type. *Nat. Commun.* **4**, 2125 (2013).
53. J. Choi, M. Ko, S. Jeon, Y. Jeon, K. Park, C. Lee, H. Lee, R. H. Seong, The SWI/SNF-like BAF complex is essential for early B cell development. *J. Immunol.* **188**, 3791–3803 (2012).
54. J. A. Gorski, T. Talley, M. Qiu, L. Puelles, J. L. R. Rubenstein, K. R. Jones, Cortical excitatory neurons and glia, but not GABAergic neurons, are produced in the Emx1-expressing lineage. *J. Neurosci.* **22**, 6309–6314 (2002).
55. T. C. Tuoc, A. Stoykova, Trim11 modulates the function of neurogenic transcription factor Pax6 through ubiquitin-proteosome system. *Genes Dev.* **22**, 1972–1986 (2008).
56. R. C. Sun, V. V. Dukhande, Z. Zhou, L. E. A. Young, S. Emanuelle, C. F. Brainson, M. S. Gentry, Nuclear glycogenolysis modulates histone acetylation in human non-small cell lung cancers. *Cell Metab.* **30**, 903–916.e7 (2019).
57. R. Narayanan, M. Pirouz, C. Kerimoglu, L. Pham, R. J. Wagener, K. A. Kiszka, J. Rosenbusch, R. H. Seong, M. Kessel, A. Fischer, A. Stoykova, J. F. Staiger, T. Tuoc, Loss of BAF (mSWI/SNF) complexes causes global transcriptional and chromatin state changes in forebrain development. *Cell Rep.* **13**, 1842–1854 (2015).
58. H. Li, B. Handsaker, A. Wysoker, T. Fennell, J. Ruan, N. Homer, G. Marth, G. Abecasis, R. Durbin; 1000 Genome Project Data Processing Subgroup, The Sequence Alignment/Map format and SAMtools. *Bioinformatics* **25**, 2078–2079 (2009).
59. H. Nguyen, C. Kerimoglu, M. Pirouz, L. Pham, K. A. Kiszka, G. Sokpor, M. S. Sakib, J. Rosenbusch, U. Teichmann, R. H. Seong, A. Stoykova, A. Fischer, J. F. Staiger, T. Tuoc, Epigenetic regulation by BAF complexes limits neural stem cell proliferation by suppressing Wnt signaling in late embryonic development. *Stem Cell Rep.* **10**, 1734–1750 (2018).
60. C. Bachmann, H. Nguyen, J. Rosenbusch, L. Pham, T. Rabe, M. Patwa, G. Sokpor, R. H. Seong, R. Ashery-Padan, A. Mansouri, A. Stoykova, J. F. Staiger, T. Tuoc, mSWI/SNF (BAF) complexes are indispensable for the neurogenesis and development of embryonic olfactory epithelium. *PLOS Genet.* **12**, e1006274 (2016).


**Acknowledgments:** We acknowledge T. Huttanus, H. Fett, U. Kunze, C. Heuchel, and U. Teichmann for expert animal care. We thank K. Jones for providing reagents, C. Dean for helpful discussions, V. Borrell and L. Valle for ferret experiment, and M. Götz for helpful inputs of study. **Funding:** This work was supported by RUB/FoRUM/F1008N-20 grant (to T.T.); TU432/1-1, TU432/3-1, and TU432/6-1 (to T.T.); AL 2231/1-1 (to M. Albert) DFG grants; Schram-Stiftung (to T.T., A.F., and M. Albert); and DFG-CNMPB (T.T., J.F.S., A.S., and A.F.). M.E. was supported by ChroNeuroRepair and advanced ERC grants, which were awarded to M. Götz. A.F. received funds from the ERC consolidator grant DEPICODE (648898), the SFB1286, and the DFG under Germany's Excellence Strategy–EXC 2067/1 39072994. **Author contributions:** C.K. performed ChIP-seq, RNA-seq, and the corresponding bioinformatics analyses. L.P. and T.T. performed most histological analyses of IUE and HDACi experiments. A.B.T., L.P., R.M., E.K., M.A., and T.T. collected human fetuses and performed analyses of expression patterns of mouse and human cortices. M.S.S. and L.K. contributed to ChIP-seq library preparation, establishment of Tbr2$^+$ cell sorting, and cell type–specific RNA-seq. Y.X., G.S., H.N., J.R., P.A.U., E.A., N.M., and B.B.-S. contributed in histological analyses, epigenome

editing, and statistical quantification. A.M. contributed to qPCR and ChIP-qPCR. V.C. performed quality control analysis and alignment of ChIP-seq and RNA-seq reads. M.A. and W.B.H. contributed in epigenome editing. M.E. contributed to *Trnp1* study. A.S., H.P.N., U.T., R.H.S., B.B.-S., and J.F.S. provided transgenic lines and research tools. J.F.S., A.S., W.B.H., M. Götz, and A.F. offered suggestions for the study. T.T. conceived the study and wrote the draft. C.K., G.S., J.F.S., M.A., M.E., A.B.T., and A.S. revised the manuscript. **Competing interests:** The authors declare that they have no competing interests. **Data and materials availability:** All RNA-seq and ChIP-seq data have been deposited in GEO under accession number GEO: GSE176194 (for BAF155cKO cortex) and GSE168298 (for $TBR2^+$ cells). All data needed to evaluate the conclusions in the paper are present in the paper and/or the Supplementary Materials.

Submitted 7 May 2020
Accepted 23 July 2021
Published 15 September 2021
10.1126/sciadv.abc6792

**Citation:** C. Kerimoglu, L. Pham, A. B. Tonchev, M. S. Sakib, Y. Xie, G. Sokpor, P. A. Ulmke, L. Kaurani, E. Abbas, H. Nguyen, J. Rosenbusch, A. Michurina, V. Capece, M. Angelova, N. Maricic, B. Brand-Saberi, M. Esgleas, M. Albert, R. Minkov, E. Kovachev, U. Teichmann, R. H. Seong, W. B. Huttner, H. P. Nguyen, A. Stoykova, J. F. Staiger, A. Fischer, T. Tuoc, H3 acetylation selectively promotes basal progenitor proliferation and neocortex expansion. *Sci. Adv.* **7**, eabc6792 (2021).

ScienceAdvances

# H3 acetylation selectively promotes basal progenitor proliferation and neocortex expansion

Cemil KerimogluLinh PhamAnton B. TonchevM. Sadman SakibYuanbin XieGodwin SokporPauline Antonie UlmkeLalit KauraniEman AbbasHuong NguyenJoachim RosenbuschAlexandra MichurinaVincenzo CapeceMeglena AngelovaNenad MaricicBeate Brand-SaberiMiriam EsgleasMareike AlbertRadoslav MinkovEmil KovachevUlrike TeichmannRho H. SeongWieland B. HuttnerHuu Phuc NguyenAnastassia StoykovaJochen F. StaigerAndre FischerTran Tuoc

*Sci. Adv.*, 7 (38), eabc6792. • DOI: 10.1126/sciadv.abc6792